Layer-Growth Kinetics on Gaseous Nitriding of Pure Iron: Evaluation of Diffusion Coefficients for Nitrogen in Iron Nitrides

MARCEL A.J. SOMERS and ERIC J. MITTEMEIJER

Models were derived for monolayer and bilayer growth into a substrate in which diffusion of the solute governs the growth kinetics, as in gas-solid reactions, for example. In the models, the composition dependence of the solute diffusivity in the phases constituting the layers was accounted for by appropriate definition of an effective diffusion coefficient for a (sub)layer. This effective diffusion coefficient is the intrinsic diffusion coefficient weighted over the composition range of the (sub)layer. The models were applied for analyzing the growth kinetics of a γ'-Fe_4N_{1-x} monolayer on an α-Fe substrate and the growth kinetics of an ε-Fe_2N_{1-z}/γ'-Fe_4N_{1-x} bilayer on an α-Fe substrate, as observed by gaseous nitriding in an NH_3/H_2-gas mixture at 843 K. The kinetics of layer development and the evolution of the microstructure were investigated by means of thermogravimetry, layer-thickness measurements, light microscopy, and electron probe X-ray microanalysis (EPMA). The effective and self-diffusion coefficients were determined for each of the nitride layers. The composition dependence of the intrinsic (and effective) diffusion coefficients was established. Re-evaluating literature data for diffusion in γ'-Fe_4N_{1-x} on the basis of the present model, it followed that the previous and present data are consistent. The activation energy for diffusion of nitrogen in γ'-Fe_4N_{1-x} was determined from the temperature dependence of the self-diffusion coefficient. The self-diffusion coefficient for nitrogen in ε-Fe_2N_{1-z} was significantly larger than that for γ'-Fe_4N_{1-x}. This was explained qualitatively, considering the possible mechanisms for interstitial diffusion of nitrogen atoms in the close-packed iron lattices of the ε and γ' iron nitrides.

I. INTRODUCTION

NITRIDING and nitrocarburizing are thermochemical surface treatments of iron and steel that bring about the following:

- a compound layer at the surface that is mainly composed of the iron (carbo)nitrides ε-$Fe_2(N,C)_{1-z}$ and γ'-$Fe_4(N,C)_{1-x}$, and
- a diffusion zone beneath the compound layer that, at the nitriding temperature (usually <863 K), consists of nitrogen interstitially dissolved in the ferrite lattice and alloying element (carbo)nitrides.

Practical application of nitriding/nitrocarburizing is based on the improvement of wear[1] and anticorrosion[2] (especially after an additional oxidation treatment) properties of the compound layer and the enhancement of the endurance limit by the diffusion zone.[1] The trend for process automation and optimization, particularly in gaseous treatments, requires an appropriate sensor to monitor the treatment parameters (gas composition and temperature) and a physical model describing the kinetics of the development of the nitrided region (=compound layer + diffusion zone). For rate control by the inward diffusion of nitrogen/carbon, a mathematical description of the diffusive flux of the interstitially dissolved elements (N, C) through the case produced is sought. This flux can be calculated using Fick's laws if the composition ranges of the phases involved, as well as the corresponding diffusion coefficients, are known.

Several attempts to model layer-growth kinetics during nitriding/nitrocarburizing have been reported in the last couple of years.[3–8] In the majority of the publications regarding this topic, a lack of data is apparent. Thus, the determination of diffusion coefficients by application of some model to relevant model experiments was not achieved.

At present, the diffusion coefficients of nitrogen and carbon in the iron (carbo)nitrides ε and γ' are not known with sufficient accuracy. This can be ascribed largely to imprecise knowledge of the homogeneity ranges of these phases. Only recently, detailed information on the composition ranges of iron nitrides has been reported[9,10] (a summary of the relevant data is given in the Appendix of the present article). Another cause for the lack of accurate diffusion coefficients is the inherent instability of iron (carbo)nitrides at the usual temperature, <863 K, and pressure, $\cong 10^5$ Pa ($\cong$1 atm), which hinders a straightforward evaluation of experimental data.

So far, diffusion coefficients for N in γ'-Fe_4N_{1-x} and in ε-$Fe_2(N,C)_{1-z}$ have been published in References 11 and 5 and 12, 13 and 5, respectively. However, the data presented in Reference 11 for γ' nitride concern self-diffusion coefficients, which have to be multiplied by the thermodynamical factor[14] to obtain values for the intrinsic diffusion coefficients, as required in models regarding growth of compound layers. This thermodynamical factor can only be calculated if the dependence of the nitrogen activity on the nitrogen content is accurately known. The published data for the diffusion coefficient of N in ε (carbo)nitride were derived from

MARCEL A.J. SOMERS, Assistant Professor, and ERIC J. MITTEMEIJER, Professor, are with the Laboratory for Materials Science, Delft University of Technology, NL-2628 AL Delft, The Netherlands.

Manuscript submitted August 25, 1993.

gaseous nitriding experiments on steel substrates[12] or from plasma-nitriding experiments on iron.[5] Such investigations hinder the extraction of fundamental data on diffusion in iron (carbo)nitrides. First, on nitriding a steel substrate, not only a nitrogen concentration-depth profile is formed over the layer produced, but also a carbon concentration-depth profile that is (partly) of opposite slope,[15] which was not considered in Reference 12. Second, diffusion coefficients for γ' and ε nitride obtained from plasma-nitriding treatments as in Reference 5 cannot be trusted, because upon plasma nitriding, concurrent with inward diffusion of nitrogen, part of the surface is sputtered away.[8] Moreover, precise determination and control of the temperature at the specimen surface during plasma nitriding is a major problem.

In the present article models describing the kinetics of monolayer (γ'-layer) growth and bilayer (ε-sublayer + γ'-sublayer) growth into a substrate are dealt with. The treatment adopts linear concentration profiles, which will be shown to be a justified approximation, and concentration-weighted intrinsic diffusion coefficients in the layer(s). The models were applied to gaseous nitriding experiments conducted at 843 K and, thus, diffusion coefficients for nitrogen in both ε and γ' nitride were obtained.

II. EVALUATION OF DIFFUSION COEFFICIENTS FROM LAYER-GROWTH KINETICS

A. *Monolayer Growth with One Diffusing Component*

The kinetics of diffusion-controlled layer growth in a binary system can be described by the shift of an interface between two phases because of a difference of the fluxes of species arriving at the interface and the fluxes of species being removed from the interface. For the case in which only one component diffuses or the diffusion of one of the two components is negligible as compared to the other, this balance of fluxes is reduced to the flux of arrival of the main diffusing component at the interface in one phase and the flux of removal of this component by diffusion into the other phase. A mathematical description for the determination of the diffusion coefficient from a growing monophase scale (*e.g.*, as formed during gas-solid interaction) has been given first by Wagner[16] for the case that

the surface and the layer/substrate interface are planar;
the substrate and layer have equal specific volumes with respect to the solvent atoms;*
the compositions at the interfaces are independent of time; and
the diffusion coefficient is independent of concentration.

*Here, the specific volume of an interstitial phase (as the iron nitrides to be considered) is defined as the volume of the unit cell divided by the number of solvent atoms per unit cell.

In the situation given in Figure 1(a), the binary phases I (substrate) and II (layer) are composed of components 1 and 2. Component 2 (solute N) is assumed to be mobile and to dissolve in both phases I and II, while component 1 (solvent Fe) is assumed to be immobile. At the surface, the concentration of solute atoms 2 is denoted by $c_{2,\mathrm{II}/s}$ (expressed as quantity per unit volume, not as a fraction). At the layer/substrate interface, the solute concentration amounts to $c_{2,\mathrm{II}/\mathrm{I}}$ in phase II and $c_{2,\mathrm{I}/\mathrm{II}}$ in phase I. For shifting the interface between the layer and substrate at ξ an infinitesimal distance $d\xi$ into the substrate within an infinitesimal lapse of time dt, an amount of $(c_{2,\mathrm{II}/\mathrm{I}} - c_{2,\mathrm{I}/\mathrm{II}}) \cdot d\xi$ of component 2 is used (shaded area in Figure 1(a)). Then, the following continuity equation holds for shifting the interface between the layer and substrate:

$$(c_{2,\mathrm{II}/\mathrm{I}} - c_{2,\mathrm{I}/\mathrm{II}}) \cdot d\xi = (j_2^{(\mathrm{II})}|_{x\uparrow\xi} - j_2^{(\mathrm{I})}|_{x\downarrow\xi}) \cdot dt = \left[\left(-D_2^{(\mathrm{II})} \cdot \frac{\partial c_2}{\partial x}\right)_{x\uparrow\xi} - \left(-D_2^{(\mathrm{I})} \cdot \frac{\partial c_2}{\partial x}\right)_{x\downarrow\xi}\right] \cdot dt \quad [1a]$$

where, $j_2^{(k)}$ is the flux of component 2 in phase k, $\partial c_2/\partial x$ is the concentration gradient of the diffusing component 2, and $D_2^{(k)}$ is the intrinsic diffusivity of component 2 in phase k.

Alternatively, for a layer growing into a substrate, growth of the layer can be expressed in terms of the flux of component 2 entering the layer at the surface and the flux of component 2 leaving the layer at the interface (Figure 1(b)). Then, the continuity equation for growth of the layer becomes (shaded area in Figure 1(b))

$$(c_{2,\mathrm{II}/\mathrm{I}} - c_{2,\mathrm{I}/\mathrm{II}}) \cdot d\xi + dW = (j_2^{(\mathrm{II})}|_{x=0} - j_2^{(\mathrm{I})}|_{x\downarrow\xi})dt = \left[\left(-D_2^{(\mathrm{II})} \cdot \frac{\partial c_2}{\partial x}\right)_{x=0} - \left(-D_2^{(\mathrm{I})} \cdot \frac{\partial c_2}{\partial x}\right)_{x\downarrow\xi}\right] \cdot dt \quad [1b]$$

where dW is the amount of solute accumulated in the layer to maintain a concentration-depth profile (Figure 1(b)). Equations [1a] and [1b] are equally valid descriptions for layer-growth kinetics. If the mass increase of a specimen in a gas-solid interaction is monitored to investigate layer growth, Eq. [1b] should be used rather than Eq. [1a], because the mass-increase rate is directly related to the flux of component 2 entering the specimen.

Recognizing the partial Gibbs free energy (=chemical potential) of component 2 as the driving force for diffusion, the intrinsic diffusion coefficient $D_2^{(\mathrm{II})}$ in Eq. [1] generally depends on concentration and can be related to the self-diffusion coefficient, $D_2^{(\mathrm{II})*}$, by[14]

$$D_2^{(\mathrm{II})} = D_2^{(\mathrm{II})*} \cdot \frac{d \ln a_2}{d \ln c_2} \quad [2]$$

where $d \ln a_2/d \ln c_2$ is the so-called thermodynamic factor and a_2 is the corresponding activity of component 2.

Now, it is assumed that the concentrations of solute at both sides of the layer/substrate interface are only a function of temperature. Then, for a given temperature, evaluation of the intrinsic diffusion coefficient $D_2^{(\mathrm{II})}$ as a function of the composition by means of layer-growth experiments is straightforward by focusing on the diffusion coefficient at the surface rather than the interface.

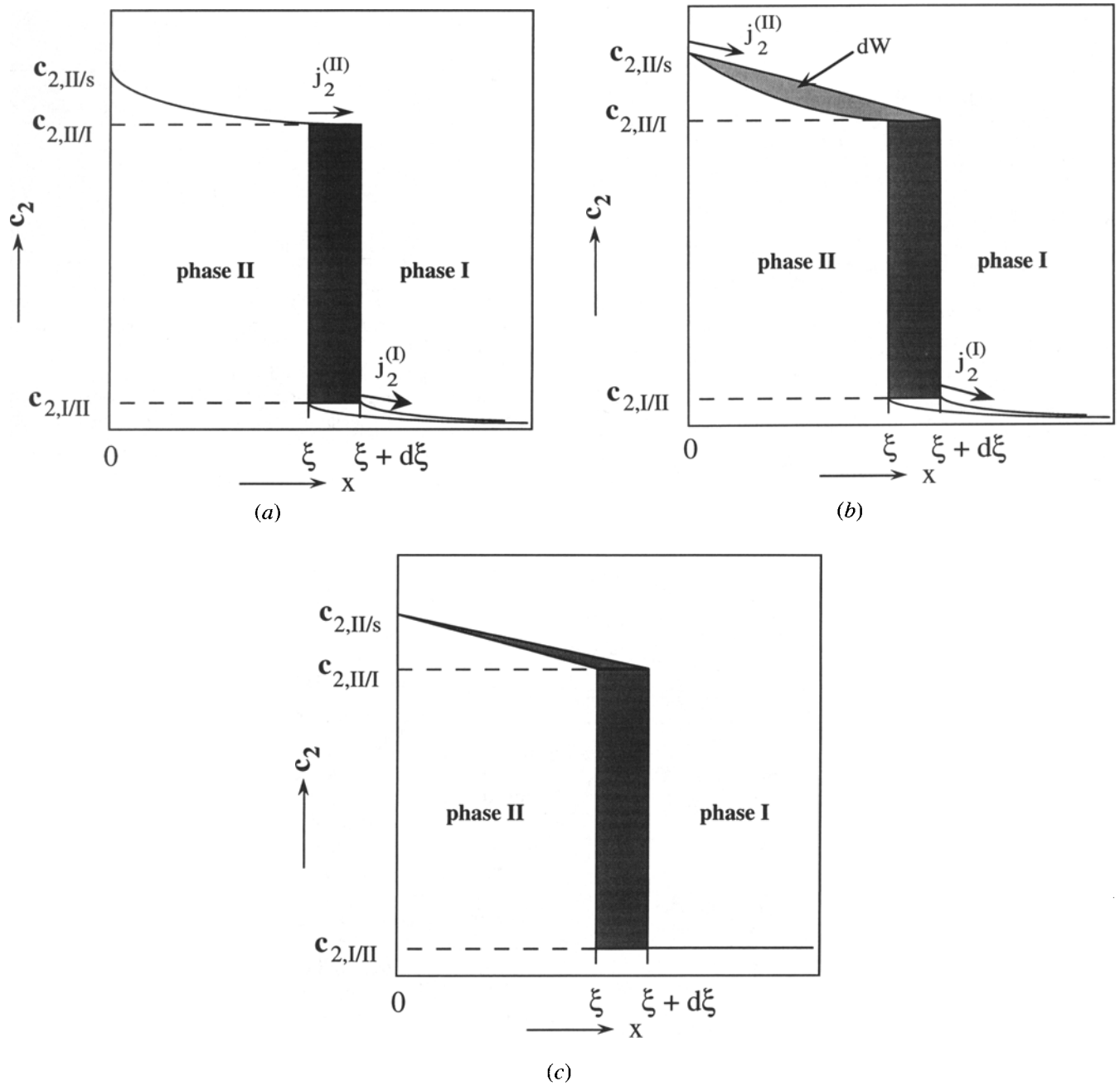

Fig. 1—(*a*) Schematic concentration-depth profile ($c_2 - x$) for diffusion-controlled growth of a monolayer (phase II) into a substrate (phase I) to illustrate Eq. [1a], where growth of the layer is related to the difference of the flux arriving at the layer/substrate interface through the layer and entering the substrate at the layer/substrate interface. (*b*) Schematic concentration-depth profile ($c_2 - x$) for diffusion-controlled growth of a monolayer (phase II) into a substrate (phase I) to illustrate Eq. [1b], where growth of the layer is related to the difference of the flux entering the layer at the surface and the flux entering the substrate at the layer/substrate interface. (*c*) Schematic concentration-depth ($c_2 - x$) profile for diffusion-controlled growth of a monolayer (phase II) into a solute-saturated substrate (phase I). The gray area indicates the amount of solute that needs to be accumulated in phase II for shifting the interface between phases II and I by a distance $d\xi$ into phase I.

At the surface, the solute concentration can be altered by adjusting the chemical potential of component 2 in the gas phase in a series of experiments at a chosen temperature, whereas at the interface, the composition, and thus the corresponding intrinsic diffusion coefficient, is fixed. Then, application of Eq. [1b] has to be preferred.

To assess the intrinsic diffusion coefficient $D_2^{(II)}$ from Eqs. [1a] or [1b], the value for the corresponding concentration gradient should be known. Moreover, employing Eq. [1b] requires that dW be known. Both parameters ($\partial c_2/\partial x$ and dW) could be calculated straightforwardly if the concentration-depth profile within the layer is known. Solving Fick's 2nd law for a known or an assumed concentration dependency of the intrinsic diffusion coefficient and the appropriate boundary conditions provides this concentration-depth profile. A different approach has been preferred in the present work.

The intrinsic diffusion coefficient for the layer can be replaced by an effective diffusion coefficient. Here, the effective diffusion coefficient is defined as the diffusion

coefficient associated with the average diffusive flux through a layer of thickness ξ with concentration range $c_{2,II/s}$ to $c_{2,II/I}$.

$$\frac{1}{\xi}\int_0^{\xi} j_2 \cdot dx = -\frac{1}{\xi}\int_{c_{2,II/s}}^{c_{2,II/I}} D_2^{(II)} \cdot dc_2$$

$$= -\frac{\langle D_2^{(II)}\rangle}{\xi}\int_{c_{2,II/s}}^{c_{2,II/I}} dc_2$$

$$= \langle D_2^{(II)}\rangle \frac{c_{2,II/s} - c_{2,II/I}}{\xi} \qquad [3a]$$

Hence

$$\langle D_2^{(II)}\rangle = \frac{1}{c_{2,II/s} - c_{2,II/I}}\int_{c_{2,II/I}}^{c_{2,II/s}} D_2^{(II)} \cdot dc_2 \qquad [3b]$$

Thus, the effective diffusion coefficient for the layer is taken as the composition-weighted intrinsic diffusion coefficient. Obviously, if the concentration profile in the layer is linear, $\langle D_2^{(II)}\rangle = D_2^{(II)}$ $(x = \xi)$ if Eq. [1a] is used and $\langle D_2^{(II)}\rangle = D_2^{(II)}$ $(x = 0)$ if Eq. [1b] is used. Replacing $D_2^{(II)}$ by $\langle D_2^{(II)}\rangle$ and adopting a linear concentration-depth profile in the layer as an estimate for the actual concentration-depth profile, the case of a monolayer growing into a *saturated* substrate by inward diffusion of component 2 on the basis of Eq. [1b] can be written as (Figure 1(c))

$$\left((c_{2,II/I} - c_{2,I/II}) + \frac{1}{2}(c_{2,II/s} - c_{2,II/I})\right) \cdot d\xi$$

$$= \langle D_2^{(II)}\rangle \cdot \frac{c_{2,II/s} - c_{2,II/I}}{\xi} \cdot dt \qquad [4]$$

Integration of this simple differential equation yields a parabolic growth equation for phase II:

$$\xi^2 = 2 \cdot \frac{(c_{2,II/s} - c_{2,II/I} \cdot \langle D_2^{(II)}\rangle \cdot t)}{\left\{(c_{2,II/I} - c_{2,I/II}) + \frac{1}{2}(c_{2,II/s} - c_{2,II,I})\right\}} + C \qquad [5]$$

with C being the integration constant reflecting the presence ($C > 0$) or absence ($C = 0$) of a layer of phase II at a chosen begin of time ($t = 0$). Thus, the effective diffusion coefficient of component 2 in phase II is readily obtained from

$$\langle D_2^{(II)}\rangle = \frac{(c_{2,II/I} - c_{2,I/II}) + \frac{1}{2}(c_{2,II/s} - c_{2,II/I})}{(c_{2,II/s} - c_{2,II/I})} \cdot k_{II} \qquad [6a]$$

where

$$k_{II} = \frac{1}{2} \cdot \frac{d(\xi^2)}{dt} = \xi \cdot \frac{d\xi}{dt} \qquad [6b]$$

denotes the parabolic growth constant.

For the case that the layer of phase II grows into an *unsaturated* semi-infinite substrate of phase I, the continuity equation analogous to Eq. [4] becomes*

*The quantity of solute that has been dissolved in phase I in the interval $d\xi$ before phase II is formed there has been ignored.[17]

$$\left((c_{2,II/I} - c_{2,I/II}) + \frac{1}{2}(c_{2,II/s} - c_{2,II/I})\right) \cdot d\xi$$

$$= \langle D_2^{(II)}\rangle \cdot \frac{c_{2,II/s} - c_{2,II/I}}{\xi} \cdot dt + D_2^{(I)}\left(\frac{\partial c}{\partial x}\right)_{x\downarrow\xi} \cdot dt \qquad [7]$$

The numerical solution of Eq. [7] has been given in Reference 19.

For the case that the substrate has a finite thickness $2L$ but can still be considered as thick as compared to the thickness of the layer, Eq. [7] can be modified to[19]

$$\left((c_{2,II/I} - c_{2,I/II}) + \frac{1}{2}(c_{2,II/s} - c_{2,II/I})\right) \cdot d\xi$$

$$= \langle D_2^{(II)}\rangle \cdot \frac{c_{2,II/s} - c_{2,II/I}}{\xi} \cdot dt +$$

$$D_2^{(I)}\left(\frac{2(c_{2,I/II} - c_0)}{L} \cdot \sum_{n=1}^{\infty} \exp\left(-\frac{(2n-1)^2 \pi^2 D_2^{(I)} \cdot t}{4L^2}\right)\right) \cdot dt \qquad [8]$$

where c_0 is the initial solute concentration in the substrate.

1. *Application to γ′-Iron Nitride Layer Growth*

The intrinsic diffusion coefficient of nitrogen in γ′-iron nitride can be calculated from the corresponding self-diffusion coefficient if the dependence of the nitrogen activity on the nitrogen concentration is known, in order to evaluate the thermodynamic factor (*cf.* discussion immediately following Eq. [2]). Nitrogen absorption isotherms, depicting the equilibrium nitrogen concentration in a phase as a function of the nitriding potential r_N imposed by an ammonia/hydrogen gas mixture ($r_N = pNH_3/pH_2^{3/2}$), can be used for this purpose, because the activity of nitrogen in γ′ nitride $a_{N,\gamma'}$ is proportional to the nitriding potential: $a_{N,\gamma'} = K'_{\gamma'} \cdot r_N$, where $K'_{\gamma'}$ contains the equilibrium constant for the dissolution of nitrogen in γ′ nitride and the fugacity coefficients (*cf.* discussion immediately following Eq. [A3]). Taking Eqs. [A1] and [A6] from the Appendix, the nitrogen concentration in γ′-nitride, $c_{N,\gamma'}$, can be written in terms of the nitrogen activity $a_{N,\gamma'}$ as

$$c_{N,\gamma'} = \frac{y_{N,\gamma'}}{N_{Av} V_{\gamma'}}$$

$$= \frac{1}{4} \cdot \frac{1}{N_{Av} V_{\gamma'}} \cdot \left\{1 + K_{\gamma'}^{WS}\left[\frac{a_{N,\gamma'}/K'_{\gamma'}}{r^0_{N,\gamma'}} - \frac{r^0_{N,\gamma'}}{a_{N,\gamma'}/K'_{\gamma'}}\right]\right\} \qquad [9]$$

where $y_{N,\gamma'}$ is the fraction of all octahedral sites in γ′-nitride that is occupied by nitrogen atoms, N_{Av} is Avogadro's number, $V_{\gamma'}$ is the volume of a unit cell of γ′-nitride per iron atom, and the other parameters have been defined for Eq. [A6] in the Appendix. Using

Eqs. [3b] and [2] for (II) = (γ') and nitrogen as component 2 (Eq. [9]) and taking $D_N^{(\gamma')*}$ and $V_{\gamma'}$ as practically independent of $c_{N,\gamma'}$, the following equation is obtained by straightforward calculus

$$\langle D_N^{(\gamma')} \rangle = \frac{1}{c_{N,\gamma'/s} - c_{N,\gamma'/\alpha}} \cdot f_{\gamma'} \cdot D_N^{(\gamma')*} \qquad [10a]$$

where $c_{N,\gamma'/s}$ and $c_{N,\gamma'/\alpha}$ are the nitrogen concentrations in γ' nitride at the surface and at the γ'/α interface, respectively. The factor $f_{\gamma'}$ contains the concentration dependence of $\langle D_N^{(\gamma')} \rangle$

$$f_{\gamma'} = \frac{1}{4N_{Av}V_{\gamma'}} \cdot \left\{ \ln \frac{r_N}{r_{N,\alpha/\gamma'}} + K_{\gamma'}^{ws} \left[\frac{r_N}{r_{N,\gamma'}^0} + \frac{r_{N,\gamma'}^0}{r_N} - \left(\frac{r_{N,\alpha/\gamma'}}{r_{N,\gamma'}^0} + \frac{r_{N,\gamma'}^0}{r_{N,\alpha/\gamma'}} \right) \right] \right\} \qquad [10b]$$

where r_N and $r_{N,\alpha/\gamma'}$ are the nitriding potentials imposed during nitriding and corresponding with the α/γ' boundary in the Lehrer diagram (Eq. [A10]), respectively, and $V_{\gamma'}$ is taken as the average value for the composition range in the layer.

From Eqs. [10a] and [6], it follows that the self-diffusion coefficient can be determined from the parabolic growth constant for the γ' monolayer, $k_{\gamma'}$:

$$k_{\gamma'} = \frac{1}{\bar{c}_{N,\gamma'}} \cdot f_{\gamma'} \cdot D_N^{(\gamma')*} \qquad [11]$$

where $\bar{c}_{N,\gamma'} = 1/2\ (c_{N,\gamma'/s} + c_{N,\gamma'/\alpha}) - c_{N,\alpha/\gamma'}$ is called the average nitrogen concentration in the γ' layer with respect to the substrate, with $c_{N,\alpha/\gamma'}$ as the nitrogen content in ferrite at the α/γ' interface.

B. *Bilayer Growth with One Diffusing Component*

Multiphase binary reaction diffusion has been dealt with at several places in the literature.[22-31] The present treatment applies to diffusion-controlled growth of a bilayer in a binary metal-interstitial system. Proceeding analogously as for the case of monolayer growth, two effective diffusion coefficients for component 2 can be defined, one for each of the two phases constituting the two layers (phase III adjacent to the surface and phase II adjacent to the substrate).

For phase III,

$$\langle D_2^{(III)} \rangle = \frac{1}{c_{2,III/s} - c_{2,III/II}} \int_{c_{2,III/II}}^{c_{2,III/s}} D_2^{(III)} \cdot dc_2 \qquad [12]$$

For phase II,

$$\langle D_2^{(II)} \rangle = \frac{1}{c_{2,II/III} - c_{2,II/I}} \int_{c_{2,II/I}}^{c_{2,II/III}} D_2^{(II)} \cdot dc_2 \qquad [13]$$

Consider Figure 2, where phase I has no solubility for component 2 or is saturated with component 2. Growth of phase III in the direction of increasing x by an infinitesimal distance $d\xi$ is associated with the accumulation in this phase of an amount of the diffusing solute represented by the darkly shaded area in Figure 2, which is the difference of the amount of component 2 diffusing through $x = 0$ into phase III and the amount of component 2 diffusing through $x = \xi$ out of phase III into phase II within a lapse of time dt. Replacing $D_2^{(III)}$ by $\langle D_2^{(III)} \rangle$ and $D_2^{(II)}$ by $\langle D_2^{(II)} \rangle$ and adopting linear concentration-depth profiles in the layers of phases III and II as estimates for the actual concentration-depth profiles, the following continuity equation results for growth of the layer of phase III into phase II (Figure 2):

$$\left((c_{2,III/II} - c_{2,II/III}) + \frac{1}{2} (c_{2,III/s} - c_{2,III/II}) \right) \cdot d\xi = \left(\langle D_2^{(III)} \rangle \cdot \frac{c_{2,III/s} - c_{2,III/II}}{\xi} - \langle D_2^{(II)} \rangle \cdot \frac{c_{2,II/III} - c_{2,II/I}}{\zeta - \xi} \right) \cdot dt \qquad [14]$$

where terms containing $(d\xi)^2$ have been neglected. Similarly, growth of phase II in the direction of increasing x by an infinitesimal distance $(d\zeta - d\xi)$ is associated with accumulation of an amount of the diffusing solute in phase II represented by the lightly shaded area in Figure 2. This quantity is the difference of the total amount of component 2 diffusing through $x = \xi$ into phase II and the amount of solute diffusing through $x = \zeta$ out of phase II into phase I within a lapse of time dt. Hence, for the case that the substrate is saturated with solute, the continuity equation for growth of the layer of phase II into the substrate (phase I) (Figure 2) reads

$$\left((c_{2,II/I} - c_{2,I/II}) + \frac{1}{2} (c_{2,II/III} - c_{2,II/I}) \right) \cdot d\zeta + \frac{1}{2} (c_{2,II/III} - c_{2,II/I}) \cdot d\xi = \left(\langle D_2^{(II)} \rangle \cdot \frac{(c_{2,II/III} - c_{2,II/I})}{\zeta - \xi} \right) \cdot dt \qquad [15]$$

where, again, terms containing $(d\xi)^2$ have been neglected.

Analogous to Eqs. [7] and [8], a term is added to the right-hand member of Eq. [15] if the substrate is not saturated with solute (also see footnote on page 60). These terms are equal to the terms in Eqs. [7] and [8] containing $D_2^{(I)}$.

A solution for the set of differential equations formed by Eqs. [14] and [15] is

$$\xi = 2A\sqrt{t}; \qquad \zeta - \xi = 2B\sqrt{t} \qquad [16]$$

where A and B are parabolic growth constants depending on the phase compositions at the interfaces and the diffusion coefficients of the diffusing component in each of the phases. It can be verified easily by substitution into Eqs. [14] and [15] that the addition of constants to the right-hand members of Eq. [16] does not provide solutions for these continuity equations (*cf.* the constant C in Eq. [5]). Hence, for the case of bilayer growth into

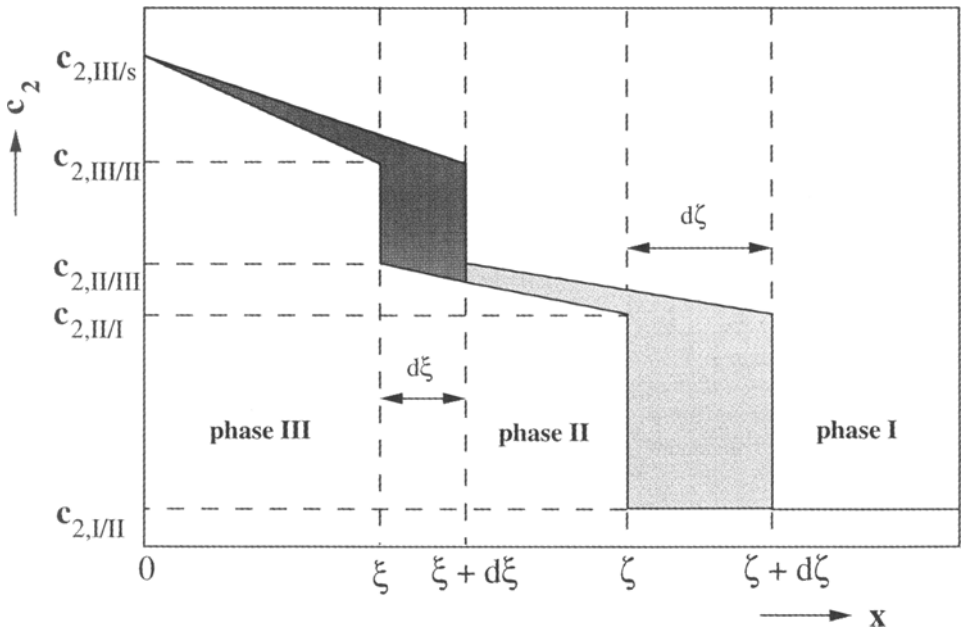

Fig. 2—Schematic concentration-depth ($c_2 - x$) profile for growth of a bilayer (constituted of sublayers of phases III and II) into a solute-saturated substrate (phase I). The dark gray area indicates the amount of solute that needs to be accumulated in phase III for shifting the interface between phases III and II by a distance $d\xi$ into phase II; the light gray area indicates the amount of solute that needs to be accumulated in phase II for shifting the interface between phases II and I by a distance $d\zeta$ into phase I.

a solute-saturated substrate, (a) both layers have to have formed instantaneously at $t = 0$ or (b) if one or both layer(s) is/are not formed instantaneously at $t = 0$, extrapolations of the two dependencies of layer thickness on time as observed after prolonged treatment should yield zero layer thickness for both layers at $t = 0$. Then, the effective diffusion coefficients of component 2 in phases II and III can be evaluated analytically from the experimentally determined parabolic growth constants as follows. Substitution of Eq. [16] in Eqs. [14] and [15] and rearrangement yields

$$\langle D_2^{(II)} \rangle = \frac{1}{c_{2,II/III} - c_{2,II/I}} \cdot [B^2\{c_{2,II/III} + c_{2,II/I} - 2\,c_{2,I/II}\} + 2AB(c_{2,II/III} - c_{2,I/II})] \quad [17a]$$

and

$$\langle D_2^{(III)} \rangle = \frac{1}{c_{2,III/s} - c_{2,III/II}} \cdot \left[A^2 \{c_{2,III/s} + c_{2,III/II} - 2c_{2,I/II}\} + 2AB \left\{ \frac{1}{2}(c_{2,II/III} + c_{2,II/I}) - c_{2,I/II} \right\} \right] \quad [17b]$$

If the growth rate of both layers cannot be described by Eq. [16] and/or if phase I is not saturated with solute, the effective diffusion coefficients for the solute in phases II and III can only be evaluated by numerical solution of Eqs. [14] and [15] (*cf.* discussion immediately following Eq. [15]).

2. *Application to ε/γ'-Iron Nitride Bilayer Growth*

For the case of ε/γ'-bilayer growth, the nitriding potential imposed by the gas mixture (only) determines the nitrogen concentration at the surface of the ε-nitride sublayer. Hence, the effective diffusion coefficient for the γ'-sublayer is the intrinsic diffusion coefficient weighted over the entire composition range of γ'-iron nitride phase at the temperature under consideration (Eq. [12]). Thus, if $\langle D_N^{(\gamma')} \rangle$ has been determined from ε/γ'-bilayer growth experiments, preferably for the case of a nitrogen-saturated ferrite substrate (*cf.* discussion immediately following Eq. [16]), the self-diffusion coefficient $D_N^{(\gamma')^*}$ can be obtained using Eq. [10], provided $c_{N,\gamma'/s}$ is replaced by $c_{N,\gamma'/\varepsilon}$ and r_N is replaced by $r_{N,\gamma'/\varepsilon}$, *i.e.*, the nitriding potential at the γ'/ε-boundary in the Lehrer diagram (Appendix, Eq. [A11]).

Using absorption isotherms for nitrogen in ε-nitride (*i.e.*, the equilibrium nitrogen concentration in ε-nitride as a function of the nitriding potential imposed by an ammonia/hydrogen gas mixture) the intrinsic diffusion coefficient for a particular nitrogen content can be expressed in terms of the self-diffusion coefficient, which is taken independent of the nitrogen concentration.

The nitrogen concentration of ε-nitride cannot be written in an explicit form as a function of the nitrogen activity, which is proportional to the nitriding potential (Eq. [A8]). Therefore, using Eq. [2] for the ε phase, it is convenient to write Eq. [12] as

$$\langle D_N^{(\varepsilon)} \rangle = \frac{1}{c_{N,\varepsilon/s} - c_{N,\varepsilon/\gamma'}} \int_{y_{N,\varepsilon/\gamma'}}^{y_{N,\varepsilon/s}} D_N^{(\varepsilon)^*} \cdot c_{N,\varepsilon} \cdot \frac{d \ln K'_\varepsilon r_N}{dy_{N,\varepsilon}} \cdot dy_{N,\varepsilon} \quad [18]$$

where $c_{N,\varepsilon/s}$ and $c_{N,\varepsilon/\gamma'}$ are the nitrogen concentrations in the ε-nitride layer at the surface and at ε/γ' interface, respectively, $y_{N,\varepsilon/s}$ and $y_{N,\varepsilon/\gamma'}$ are the corresponding nitrogen contents expressed as the occupied fractions of

the available sites for nitrogen atoms (Appendix), and K'_ε contains the equilibrium constant for the dissolution of nitrogen in ε nitride and the fugacity coefficients (Eq. [A3]). Substituting Eq. [A1], $c_{N,\varepsilon} = y_{N,\varepsilon}/N_{Av}V_\varepsilon$, and Eq. [A8] in Eq. [18] and assuming $D_N^{(\varepsilon)*}$ and V_ε are practically independent of $c_{N,\varepsilon}$ (V_ε is taken as the average value for the composition range in the layer under consideration), the following equation is obtained

$$\langle D_N^{(\varepsilon)} \rangle = \frac{1}{y_{N,\varepsilon/s} - y_{N,\varepsilon/\gamma'}} \cdot f_\varepsilon \cdot D_N^{(\varepsilon)*} \qquad [19a]$$

where f_ε contains the concentration dependence of $\langle D_N^{(\varepsilon)} \rangle$

$$f_\varepsilon = -4.0\{y_{N,\varepsilon/s}^2 - y_{N,\varepsilon/\gamma'}^2\} + 27.4\{y_{N,\varepsilon/s}^3 - y_{N,\varepsilon/\gamma'}^3\} \qquad [19b]$$

No correction has been carried out for differences in the molar volumes of the phases in sublayer(s) and substrate. It was verified that application of the correction procedure as given in Reference 31 to the present case of γ' monolayers and ε/γ' bilayers leads to negligible corrections.

III. EXPERIMENTAL

A. *Specimen Preparation*

Rectangular specimens (15 × 9 × 1.0 mm) were cut from a cold-rolled slab of pure iron (Materials Research Société Anonyme, Toulouse, France) of composition: 100 ppm C, 650 ppm O, 3 ppm N, <1 ppm Al, 8 ppm Cr, 2 ppm Mn, <1 ppm Si, balance Fe. Prior to nitriding, the samples were recrystallized for 1 hour at 923 K in Ar and additionally ground and polished down to 0.8 mm thickness. The final pretreatment was etching for about 2 minutes in Nital 2 pct (2 vol pct HNO_3 in ethanol).

Gaseous nitriding was performed in a vertical quartz-tube furnace at 843 ± 1 K. Gases NH_3 (Matheson, minimum 99.96 vol pct pure) and H_2 (Hoek–Loos, minimum 99.90 vol pct pure) were led through BTS catalyst and soda lime for deoxidation and drying, respectively. The composition of the gas mixtures was adjusted with mass-flow controllers (Brooks 5810–5835). The linear velocity of the gas mixture through the tube of the furnace, as measured at room temperature, was 3 mm · s^{-1}. The ammonia/hydrogen gas mixtures contained 30 vol pct NH_3 and 56.1 vol pct NH_3 for the production of γ' monolayers and ε/γ' bilayers, respectively. Specimens were weighed prior to and after nitriding with a mechanical microbalance (Mettler; sensitivity = 1 μg). After nitriding, the samples were cooled moderately fast in the respective NH_3/H_2 gas mixtures by pulling them into a cold part of the furnace. This led to the precipitation of both γ'-Fe_4N_{1-x} and α''-$Fe_{16}N_2$ in the diffusion zone of the α-Fe substrate during cooling.

B. *Lightmicroscopical Analysis*

The specimens were electrolytically sheathed with a nickel layer in a Watts bath (at 345 K) in order to prevent damaging and rounding off at the edges during subsequent preparation for lightmicroscopical investigation. Cross sections were ground and polished (last polishing step: 0.25 μm diamond paste) and etched in either Nital 1 pct or Nital 1 pct modified with HCl.[32,15] The latter etchant attacks the nitride layer more severely than the former, leading to a small height difference in the cross section at the layer/substrate interface but also to exaggeration of the dimensions of the pores in the layer.

Layer-thickness measurements were carried out in bright field, applying monochromatic illumination (λ = 580 nm) for a sharp definition of the interfaces. Each value for the layer thickness given is the average of 40 measurements at equidistantly spaced positions parallel to the surface of the layer and represented as the 95 pct confidence interval of these measurements.

C. *Electron-Probe X-Ray Microanalysis*

A JEOL* JXA 733 electron probe X-ray microanalyzer equipped with four wavelength-dispersive spectrometers and a fully automated analysis system (TRACOR NORTHERN** TN5500 and TN5600) was used for determination of nitrogen and iron contents in the ε/γ' bilayers. The homogeneity range of the γ'-monolayers was too small (only a few tenths atomic percent) to allow quantitative determination of the composition-depth profile by EPMA within a reasonable measurement time.[33] In order to obtain a sufficient density of data points to assess the nitrogen-depth profile for the ε/γ' bilayers, the measurements were carried out in a cross section at points 1 μm apart along lines inclined with respect to the surface. The intensities of nitrogen, iron, carbon, and nickel K_α radiations as excited by an incident electron beam of 10 keV were measured. The C K_α intensities were used to correct for surface contamination by carbon deposited during the measurement, as this strongly influences the intensity of the N K_α radiation; Ni K_α intensities were used to assess the location of the interface between the layer surface and the electrolytically deposited Ni layer. For quantification, the measured intensities were compared with the corresponding intensities of standard specimens, *i.e.*, γ'-Fe_4N_{1-x} (x = 0.0024[33]), θ-Fe_3C, pure Fe, and pure Ni. The N, C, and Fe contents were evaluated from the intensity ratios (sample *vs* standard) by applying the modified $\phi(\rho z)$ approach.[34]

*JEOL is a trademark of Japan Electron Optics, Ltd., Tokyo.

**TRACOR NORTHERN is a trademark of Noran Instruments, Inc., Middleton, WI.

IV. FORMATION AND GROWTH OF IRON-NITRIDE LAYERS

A. *γ'-Fe_4N_{1-x} Monolayer on α-Fe*

The weight gain per unit area by nitrogen uptake during nitriding at 843 K in the 30 vol pct NH_3/70 vol pct

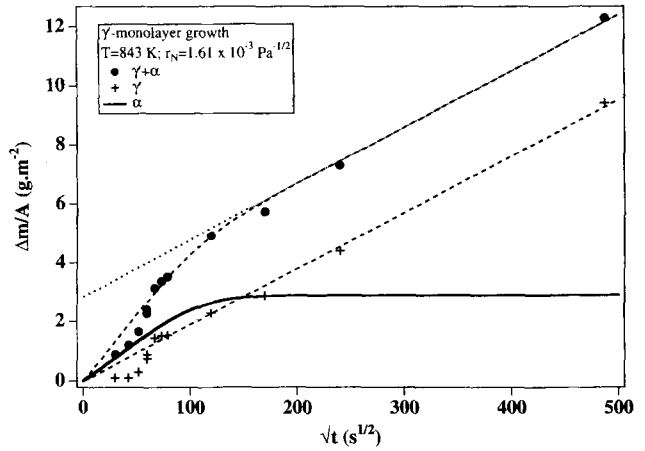

(*a*)

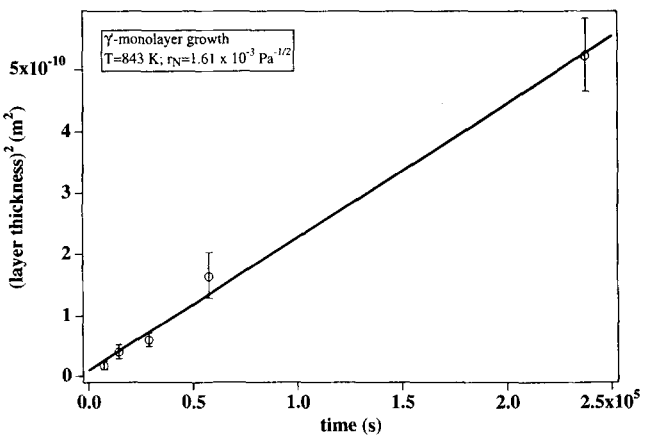

(*b*)

Fig. 3—(*a*) Weight increase per unit area ($\Delta m/A$) as a function of the square root of nitriding time (t) for growth of a γ'-Fe_4N_{1-x} layer into an initially nitrogen-free substrate of α-Fe. Nitriding conditions: T = 843 K, and r_N = 1.61 × 10^{-3} $Pa^{-1/2}$. Solid points denote experimental data; the drawn line indicates the calculated weight increase associated with the dissolution of nitrogen in the ferrite substrate; crosses denote weight increase resulting from development of the γ'-nitride layer only. (*b*) Squared thickness of the γ'-nitride layer *vs* nitriding time.

H_2 gas mixture is shown in Figure 3(a); the thickness of the growing γ'-nitride layer is depicted in Figure 3(b).*

*Weight-gain and layer-thickness results are presented in different ways in the present article, *i.e.*, weight gain *vs* $\sqrt{t}$ and layer thickness squared *vs* t. In the first plot, additivity can be demonstrated for weight gains associated with saturation of the substrate and with layer growth (Ref. 49). In the second plot, additivity of time (not $\sqrt{t}$) can be applied simply for investigating the occurrence of possible incubation times for layer development (Eq. [5]).

It is concluded that on prolonged nitriding, a parabolic weight increase and a parabolic layer growth take place. The onset of a parabolic time dependence occurs at an earlier stage of nitriding for the thickness of the γ' layer than for the total weight gain. However, the total weight gain determined contains both the weight gain because of dissolution of nitrogen in the ferrite substrate and the weight gain associated with γ'-layer development. The weight gain by dissolution of nitrogen in the ferrite matrix was calculated using Eq. [4.20] of Reference 18 (saturation of an initially solute-free plane sheet with equal and constant surface concentrations) and is also given in Figure 3(a) (full line). The data used in this calculation were as follows: nitrogen solubility in α-Fe in equilibrium with γ'-nitride 516.4 Mol · m^{-3} at 843 K (Appendix) and the diffusion coefficient of nitrogen in α-Fe, 9.93 $m^2 \cdot s^{-1}$ at 843 K.[35] The calculated weight increase by nitrogen dissolution in the ferrite substrate was subtracted from the measured total weight increase. This yielded the values represented by the crosses in Figure 3(a), which represent the weight increase only resulting from the development of γ' nitride at the surface.

The nucleation of iron nitride at the gas-solid interface takes place after the nitrogen content at this particular interface exceeds a critical value. The accumulation of nitrogen at the gas-solid interface is the net result of a competition between the supply of nitrogen from the gas phase and the removal of nitrogen by diffusion into the substrate. This explains the occurrence of an incubation time for nitride nucleation. A mathematical description for the nucleation of γ'-Fe_4N_{1-x} at an α-Fe surface was provided in Reference 36 and the incubation time for γ'-nitride nucleation thus predicted was shown to be in fair agreement with the experimental findings. Application of this model for the present nitriding conditions provides an incubation time for nitride nucleation of 350 seconds. The time where the measured total weight gain (the dots in Figure 3(a)) deviates from the calculated weight gain resulting from dissolution of nitrogen in ferrite (full line in Figure 3(a)) indeed indicates a short incubation time for γ'-nitride nucleation of the order of magnitude calculated.**

**Note that the initial increase of the surface nitrogen concentration was omitted in the calculation of the curve in Figure 1 depicting nitrogen saturation of α-Fe. Further, the reduction in thickness of the remaining substrate due to layer development was neglected.

Lightmicroscopical investigation of the nitrided surface showed that the onset of the parabolic regime, as exhibited in Figure 3(a) (crosses) and Figure 3(b), at a treatment time of about 2 hours coincides with isolation of the ferrite matrix from the gas phase by a nitride layer.

Before an isolating γ' layer has formed, the weight increase resulting from the development of γ' nitride proceeds faster than according to the parabolic relationship holding for longer treatment times. This can be explained as follows. Prior to isolation of the substrate from the nitriding atmosphere, in addition to the one-dimensional in-depth growth of the nuclei that prevails in the parabolic-growth stage, lateral growth of the nuclei occurs and nucleation continues. Both mechanisms can contribute to a larger increase of the total volume of nitride per unit time than results from inward growth of the nitride layer. Further, in this stage of layer development, nitrogen can be supplied to a growing γ' nucleus *via* ferrite. Because the homogeneity ranges of γ' and α are of comparable magnitude under the present conditions and the diffusion coefficient of N in α-Fe is considerably larger than that of N in γ'-Fe_4N_{1-x}, this bypass effect can lead to faster growth of γ' than by transport

of nitrogen to the α/γ' interface through the γ' phase only.

B. ε-Fe_2N_{1-z}/γ'-Fe_4N_{1-x} Bilayer on α-Fe

The weight gain per unit area by nitrogen uptake during nitriding at 843 K in the 56.1 vol pct NH_3/43.9 vol pct H_2 gas mixture is shown in Figure 4(a); the thicknesses of the growing ε and γ' sublayers are depicted in Figure 4(b). It is concluded that although parabolic time dependencies apply for the layer thicknesses, a parabolic time dependence does not hold for the total weight gain of the specimen (but it does hold after some time for the weight gain associated only with nitride development). The weight gain calculated for dissolution of nitrogen in α-Fe is also given in Figure 4(a) (full line; *cf.*, Section IV–A). The incubation time for γ'-nitride nucleation at the iron surface was calculated to be only 41 seconds under the present nitriding conditions (*cf.*, Section IV–A). Lightmicroscopical analysis showed that layer formation starts with the nucleation of γ' nitride on iron followed by the nucleation of ε-nitride on top of γ' nuclei before isolation of the substrate from the gas mixture by (only) a γ' layer has taken place (Figure 5(a)). An isolating ε/γ' bilayer had developed after nitriding for about 35 minutes (Figure 5(b)). This moment coincides with the onset of the parabolic time dependence of the weight gain resulting only from iron-nitride development, as indicated by the straight line through the crosses in Figure 4(a).

For treatment times exceeding 300 minutes, a positive deviation from the parabolic time dependencies was found for both weight gain (crosses) and layer thickness (Figure 4). Light microscopy showed appreciable porosity at this stage in the ε part of the bilayers (Figure 5(c)). This effect can explain the previously mentioned deviations from the straight lines in Figure 4.

Porosity is caused by the instability of iron nitrides with respect to decomposition in pure iron and nitrogen

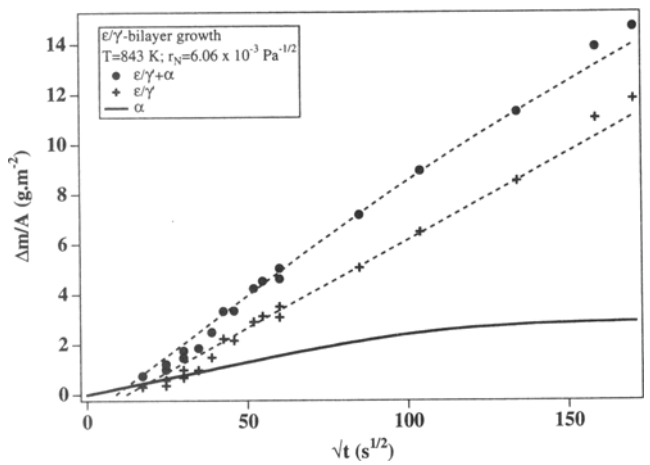

(*a*)

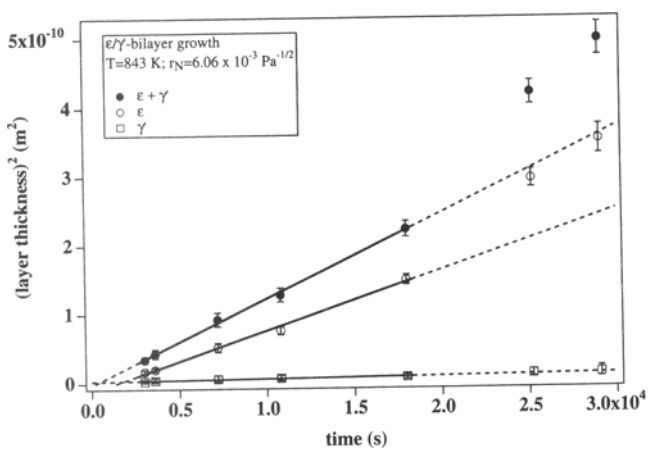

(*b*)

Fig. 4—(*a*) Weight increase per unit area ($\Delta m/A$) as a function of the square root of nitriding time (t) for growth of an ε-Fe_2N_{1-z}/γ-Fe_4N_{1-x} layer into an initially nitrogen-free substrate of α-Fe. Nitriding conditions: T = 843 K and $r_N = 6.06 \times 10^{-3}$ $Pa^{-1/2}$. Solid points denote experimental data; the drawn line indicates the calculated weight increase associated with the dissolution of nitrogen in the ferrite substrate; crosses denote weight increase resulting from the development of the ε/γ'-nitride layer only. (*b*) Squared thickness of the ε- and γ'-nitride layer *vs* nitriding time.

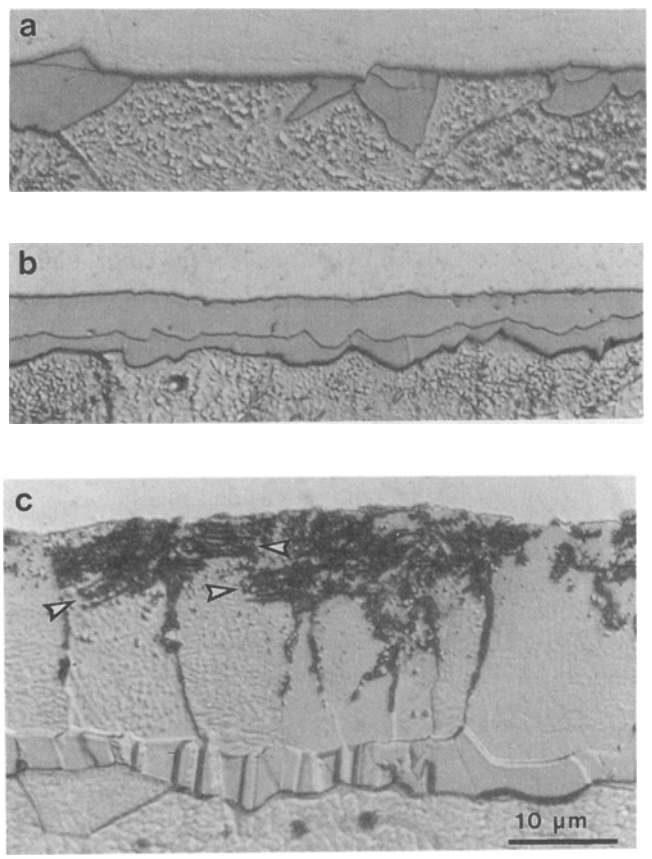

Fig. 5—Light-optical micrographs representing the evolution of the ε/γ'-nitride layer at T = 843 K and $r_N = 6.06 \times 10^{-3}$ $Pa^{-1/2}$: (*a*) after 15 minutes: dual phase nuclei ε/γ' have developed at the surface (etched in Nital 1 pct; obliquely illuminated with monochromatic light: λ = 530 nm); (*b*) after 35 minutes: an isolating dual phase ε/γ'-nitride layer has developed at the surface (etched in Nital 1 pct; obliquely illuminated with monochromatic light: λ = 530 nm); and (*c*) after 8 hours: porosity has developed in the surface-adjacent part of the ε-nitride sublayer, predominantly along grain boundaries, but also intragranularly along lines (see arrows), suggesting that intragranular nucleation of pores occurs preferably along specific crystallographic planes (etched in modified Nital 1 pct; obliquely illuminated with monochromatic light: λ = 530 nm).

gas at nitriding temperature and pressure; the equilibrium nitrogen partial pressure of the iron nitrides being of the order of 10^{10} to 10^{11} Pa at 843 K. An apparent nitrogen partial pressure of this magnitude is imposed by the ammonia/hydrogen gas mixture *at the surface* of the nitride layer. Hence, iron nitrides are stable there. However, in the interior of the nitride layer, an imposed chemical potential of this magnitude is absent and the nitrides tend to decompose in order to arrive at thermodynamic equilibrium, leading to the precipitation of N_2 gas in the layer. Most N_2 pores are observed just below the layer surface, because that is where the highest nitrogen supersaturation occurs and because this is the oldest part of the nitride layer (for the layer grows into the substrate). Pores are first observed at grain boundaries, because these provide easy nucleation sites. The occurrence of porosity is not confined to ε nitride; it has also been reported for γ' nitride [33] and N austenite.[37]

The consequences of porosity for the specimen weight gain and the nitride-layer thickness can be understood as follows. High internal N_2 pressure in closed pores leads to blowing up of the outer part of the layer (in Figure 5(c) grains exhibiting severe porosity protrude from the specimen surface). This causes, in particular, an additional layer thickness increase (Figure 4(b)) that is not a result of phase growth by inward diffusion of nitrogen. Further, by coalescence of individual pores, channels are established, connecting the outer atmosphere with the interior of the layer. Then, the nitriding potential is also imposed up to a certain depth at these freshly created channel surfaces. This leads to additional weight increase (Figure 4(a)) and modification of the concentration-depth profile.[38]*

*The first appearance and the subsequent evolution of porosity are largely determined by the purity of the iron used. Nitrides formed on very pure iron become porous relatively quickly, whereas in the present relatively oxygen-rich iron, porosity was observed relatively late. The segregation of impurities at grain boundaries may provide an explanation for delayed/retarded nucleation of pores at these locations.

Further, for relatively long nitriding times, loss of nitrogen dissolved in ε nitride by N_2 development can lead to transformation of ε-nitride (back) to γ' nitride, or even α-Fe. In the surface-adjacent region, ε nitride is maintained, because the nitriding potential of the gas mixture is imposed there (*cf.*, the austenite → ferrite (back) transformation of porous (thick) foils).[37]

As compared to the results for γ'-monolayer growth, the onset of both parabolic weight increase and parabolic layer thickness increase for ε/γ'-bilayer growth occurs sooner after the start of nitriding. This can be explained as follows.

First, the higher nitriding potential used for formation of the ε/γ' bilayer brings about a faster accumulation of nitrogen at the ferrite surface and, thus, earlier and more dense nucleation of γ'-nitride than for the nitriding potential used for the formation of the γ' monolayer. As a consequence, less lateral growth of the γ' nuclei is required for complete coverage of the surface with nitride.

Second, after exceeding the maximum nitrogen solubility of γ' nitride at the surface of a γ'-nitride nucleus, ε nitride nucleates on top of it. The homogeneity range of ε nitride is much broader than that of γ' nitride. Further, the *effective* diffusion coefficients for nitrogen in ε-and γ'-nitride layers are about equal (see Section V). Then, the flux of nitrogen through an ε layer will be larger than that through a γ' layer. Consequently, the growth rate of the ε sublayer and thus the ε/γ' bilayer will be larger than for the γ' monolayer. Because the γ' sublayer is partly consumed by the faster growing ε-sublayer, a thinner γ' layer results than for the case of a γ' monolayer.

V. INTERPRETATION OF GROWTH KINETICS OF IRON-NITRIDE LAYERS

Prior to the determination of diffusion coefficients of nitrogen in γ'-nitride layers and in ε-nitride layers by application of the models given in Section II, the validity of approximating the composition-depth profile in the growing mono- and bilayers by linear nitrogen concentration-depth profiles in each of the nitride phases was verified.

It has been shown[33,38] that the surface and interface compositions for a γ'-nitride layer growing into an α substrate agree within experimental accuracy with the equilibrium data derived from absorption isotherms (as given in Reference 9) valid for γ' nitride in equilibrium with ammonia/hydrogen gas mixtures (at the surface) and the Fe-N phase diagram (at the γ'/α interface). Also, a linear nitrogen concentration-depth profile appears to be a good approximation for a solid (nonporous) layer (Figure 6(a) in Reference 38). Such a verification has not yet been performed for ε nitride (sub)layers. The nitrogen-concentration depth profile for the bilayer obtained after 2 hours of nitriding as determined by EPMA is given in Figure 6. It can be concluded that a linear nitrogen concentration-depth profile is a good approximation for the composition-depth profile in the ε sublayer. Nitrogen contents at the surface and at the ε/γ'

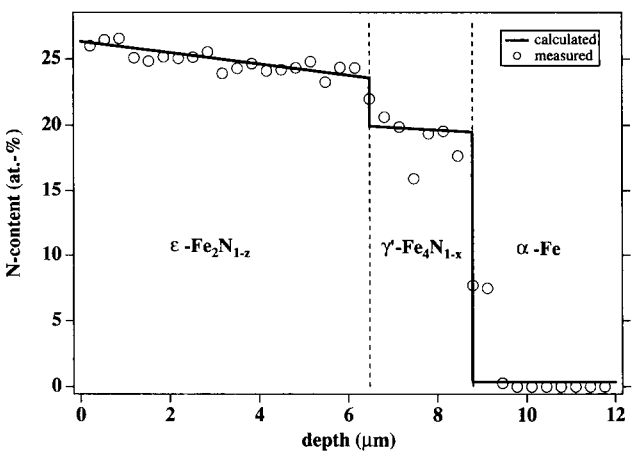

Fig. 6—Composition-depth profile for an ε/γ' bilayer after nitriding for 120 minutes at T = 843 K and $r_N = 6.06 \times 10^{-3}$ Pa$^{-1/2}$. The nitrogen content (in at. pct N) was determined with EPMA in a cross section along a line inclined with respect to the specimen surface in order to enhance the number of measurement locations, as compared to measurement along a line perpendicular to the surface. The drawn line gives the nitrogen-depth profile calculated from the data in the Appendix assuming a linear nitrogen-depth profile in each of the sublayers and thermodynamic equilibrium at the surface and sublayer interfaces (Table I displays the surface and interface compositions).

interface can be assessed by extrapolation to the corresponding positions of a straight line obtained by least-squares fitting to the experimental composition-depth profile in the ε sublayer. The values thus obtained are given in Table I and compared with those calculated from the data in the Appendix. The calculated compositions at the other interfaces are given in Table I, too. Within experimental accuracy the experimental surface and interface compositions for the ε phase agree with those obtained from the absorption isotherm (at the surface) and the Fe-N phase diagram (at the ε/γ' interface).

A. γ'-Fe_4N_{1-x} Monolayers: Diffusion Coefficient of Nitrogen in γ'-Nitride

Because the ferrite substrate is saturated with nitrogen for the major part of the parabolic growth stage of an isolating γ' layer (Figure 3(a) and Section II), the effective diffusion coefficient for nitrogen in γ'-Fe_4N_{1-x}, $\langle D_N^{(\gamma')}\rangle$ could be obtained directly from the slope of the straight line in Figure 3(b), applying Eq. [6a]. In accordance with the preceding discussion, the compositions at the gas/γ' and γ'/α interfaces are taken as those corresponding with local thermodynamic equilibrium: the nitrogen concentration in γ' at the gas/γ' interface is given by the absorption isotherm and the nitrogen concentrations in γ' and α at the γ'/α interface are given by the phase boundaries $(\alpha + \gamma')/\gamma'$ and $\alpha/(\alpha + \gamma')$ in the Fe-N phase diagram, respectively. All relevant data are given in the Appendix. It is obtained $\langle D_N^{(\gamma')}\rangle = 5.97 \times 10^{-14}$ m$^2 \cdot$ s^{-1} at 843 K.

The self-diffusion coefficient can be evaluated using Eq. [11]. The parabolic rate constant $k_{\gamma'}$ is given as a function of $f_{\gamma'}/\bar{c}_{N,\gamma'}$ (Eq. [11]) in Figure 7, using the result of the present experiments as well as data from Reference 11 that were re-evaluated according to the present model. The value for $V_{\gamma'}$ used for the calculation of $f_{\gamma'}$ is the value corresponding with the average nitrogen concentration in the layer. Linearity of the dependence of $k_{\gamma'}$ on $f_{\gamma'}/\bar{c}_{N,\gamma'}$ gives credence to the assumption that the self-diffusion coefficient of nitrogen in γ' nitride does not depend on the nitrogen content (within experimental accuracy). Values for the self-diffusion coefficients were obtained from the slopes of the straight lines through the data, including the origin, and are collected in Table II. Assuming that the temperature dependence of the self-diffusion coefficient obeys an Arrhenius-type behavior, Figure 8 is obtained. The present experiments appear to be very well compatible with those from Reference 11. The data in Figure 8 can be described by

$$\ln D_N^{(\gamma')*} = -\frac{91.4 \times 10^3}{RT} - 21.7 \qquad [20]$$

where $D_N^{(\gamma')*}$ is given in m$^2 \cdot$ s^{-1}, R is the universal gas

Table I. Nitrogen Contents (in At. Pct N) at the Surface and at the Interfaces of an ε/γ' Bilayer Prepared at T = 843 K and $r_N = 6.06 \times 10^{-3}$ Pa$^{-1/2}$*

Position	N Content (At. Pct N) Calculated	N Content (At. Pct N) Experimental
Surface	26.34	25.99
ε/γ'-interface	23.59	23.65
γ'/ε-interface	19.923	—
γ'/α-interface	19.479	—
α/γ'-interface	0.365	—

*Contents denoted "calculated" were calculated for the present nitriding conditions from data given in the Appendix for the absorption isotherm (at the surface) and the Fe-N phase diagram (at the interfaces); contents denoted "experimental" were obtained for the ε-sublayer by extrapolation to the surface and interface positions of the straight line obtained by least-squares fitting to the composition data of the ε sublayer (Fig. 6).

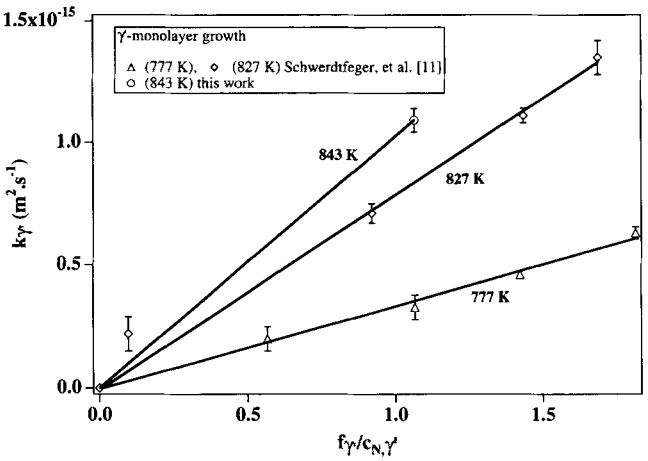

Fig. 7—The parabolic rate constant $k_{\gamma'}$ *vs* the concentration factor $f_{\gamma'}/\bar{c}_{N,\gamma'}$ (Eq. [11]) for various temperatures.

Table II. Self-Diffusion Coefficients for Diffusion of Nitrogen in γ'-Fe_4N_{1-x} and ε-Fe_2N_{1-z}, $D_N^{(\gamma')\dagger}$ and $D_N^{(\varepsilon)*}$.

T (K)	$D_N^{(\gamma')*}$, $D_N^{(\varepsilon)*}$ (10^{-16} m$^2 \cdot$ s^{-1})	Reference
777	3.37 (γ')	11
827	7.92 (γ')	11
843	10.2 (γ')	this work
843	126 (ε)	this work

†See the slopes of the straight lines in Fig. 7.

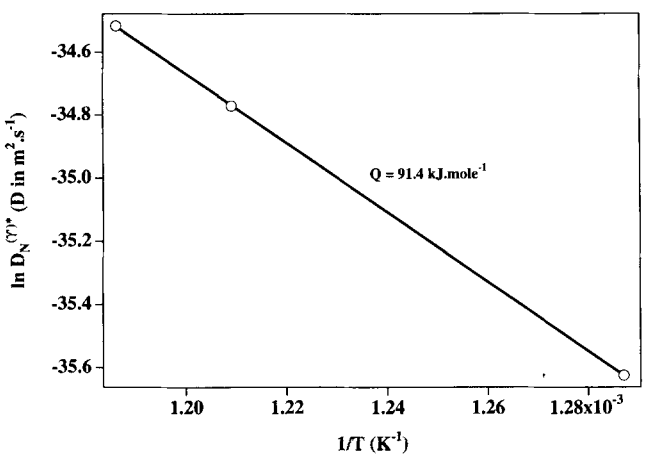

Fig. 8—Arrhenius-type plot for the self-diffusion coefficient of nitrogen in γ' nitride, $D_N^{(\gamma')*}$ (*cf.* Table II). The activation energy Q was determined from the slope of the straight line.

constant (= 8.3143 J · mole^{-1} · K^{-1}), and T is expressed in Kelvin. Hence, the activation energy for diffusion of nitrogen in γ'-nitride as determined from layer-growth experiments is 91.4 kJ · mole^{-1}. This value compares favorably with the value for the activation energy for diffusion of nitrogen in γ-Fe containing an appreciable amount of (disordered) nitrogen: Q = 90 kJ · mole^{-1} for 9.5 at. pct N.[39]**

**In a previous article, the precipitation of ferrite in γ'-Fe_4N_{1-x} on annealing was found to be governed by an activation energy of 166 kJ · mole^{-1}.[40] This activation energy was ascribed to the diffusion of nitrogen in γ' nitride. According to our present opinion, the rate-determining step during the precipitation of ferrite in γ' nitride is associated with the nucleation of ferrite, *e.g.*, the transformation of the fcc to the bcc iron lattice (from γ' to α) and/or iron (pipe) diffusion (*cf.* Ref. 39), rather than the removal of nitrogen by diffusion in γ' nitride.

The intrinsic diffusion coefficient of nitrogen in γ' nitride depends strongly on the nitrogen concentration, because the thermodynamical factor changes strongly with the composition. The effective diffusion coefficient for a γ'-nitride layer at 843 K, taken as the *intrinsic* diffusion coefficient of nitrogen in γ' nitride weighted over the composition range of the layer concerned, changes by a factor of 2 within the homogeneity range of the γ' phase at this temperature, which is only about 0.5 at. pct.

B. ε-Fe_2N_{1-z}/γ'-Fe_4N_{1-x} Bilayers

Although the thicknesses of the sublayers composing the bilayer appear to grow parabolically in time, the diffusion coefficient for ε nitride cannot be derived straightforwardly from the present experiments by application of Eq. [17], because extrapolation of the parabolic dependencies to $t = 0$ does not yield zero thickness for both sublayers (Figure 4(b) and discussion immediately following Eq. [16]). This is caused mainly by the substrate being not saturated in the time range considered (Figure 4(a)). Hence, the experimentally observed parabolic thickness increase for both sublayers (Figure 4(b)) within the restricted range is fortuitous. Nevertheless, to illustrate the effect of a saturating substrate on the value of the effective diffusion coefficients as evaluated from the apparent parabolic dependencies in Figure 4(b), Eq. [17] will be applied. From the slopes of the straight lines in Figure 4(b), it is obtained that $A = 5.07 \times 10^{-8}$ m · s$^{-1/2}$ and $B = 5.79 \times 10^{-9}$ m · s$^{-1/2}$ (*cf.*, Eq. [16]). Then, from Eq. [17] and the concentration data in the Appendix, it is obtained that $\langle D_N^{(\varepsilon)} \rangle = 4.3 \times 10^{-14}$ m^2 · s^{-1} and $\langle D_N^{(\gamma')} \rangle = 2.8 \times 10^{-14}$ m^2 · s^{-1}. The expected value for $\langle D_N^{(\gamma')} \rangle$ is calculated from the self-diffusion coefficient given by Eq. [20] and applying Eq. [10]. It is obtained that $\langle D_N^{(\gamma')} \rangle = 7.66 \times 10^{-14}$ m^2 · s^{-1}. Hence, application of Eq. [17] in the case of bilayer growth yielded a value for $\langle D_N^{(\gamma')} \rangle$, which is much too small because of ignoring a flux of nitrogen atoms into the substrate. Therefore, for the present bilayer experiments, the diffusion coefficients for nitrogen in each of the nitride sublayers can only be determined by numerically solving Eqs. [14] and [15]. This is dealt with in Section VI.

VI. SIMULATION OF LAYER-GROWTH KINETICS

The purpose of the simulation of layer-growth kinetics is twofold. First, the influence of the dissolution of nitrogen into the substrate on monolayer-growth kinetics will be demonstrated for the case of γ'-monolayer growth under the present nitriding conditions. Second, it will be shown how an effective diffusion coefficient for nitrogen in the ε-nitride sublayer can be determined for the case of ε/γ' bilayer growth on a substrate simultaneously saturating with nitrogen.

To this end, the differential equations (Eqs. [4], [7], and [8]) for monolayer growth and those (Eqs. [14] and [15]) for bilayer growth, including the appropriate terms for solute dissolution in the substrate (see text immediately following Eq. [15]), were transformed into finite difference form. In the calculations chosen, values for the diffusion coefficients were adopted and nitrogen concentration data (in mole · m^{-3}) at the interfaces were taken in conformity with data in the Appendix. Time was incremented such that equidistant intervals for $\sqrt{t}$ resulted. For each time step, the associated thickness increment(s) of the monolayer or of each of the sublayers in the bilayer were calculated. The layer-thickness values inserted in the equations were those obtained by augmenting the layer thickness used in the preceding step with the increase calculated in the preceding step. Consequently, for the first step in the calculations a nonzero layer thickness at a specific time had to be chosen. This initial point is referred to as the starting point hereafter. The thickness increase per step has to be adequately small to obtain sufficiently accurate results. It was verified that a smaller time increment in the calculations did not lead to a significantly different outcome.

A. γ'-Fe_4N_{1-x} Monolayer Growth

The simulations of γ'-monolayer growth serve to investigate the effect of the dissolution of nitrogen in the ferrite substrate on the layer-growth kinetics. The value for the diffusion coefficient for nitrogen in γ' nitride was taken as $\langle D_N^{(\gamma')} \rangle = 5.97 \times 10^{-14}$ m^2 · s^{-1} (see the preceding result). The starting point for all layer-growth simulations was chosen such that, for the case of growth into a solute-saturated substrate, a zero layer thickness resulted from extrapolation to $t = 0$ of the calculated parabolic relationship, *i.e.*, conforming to $C = 0$ in Eq. [5]. The results of the calculations for the cases of γ'-nitride layer growth (1) on a nitrogen-saturated ferrite substrate, (2) on a semi-infinite unsaturated ferrite substrate, and (3) on an unsaturated ferrite substrate of finite thickness ($2L = 8 \times 10^{-4}$ m) are shown in Figure 9. For the case of a γ' layer growing into a semi-infinite initially pure ferrite substrate, a parabolic time dependence of the layer thickness is obtained, just as for the case of γ'-layer growth into a nitrogen-saturated ferrite substrate. Clearly, the flux of nitrogen from the γ' layer into the unsaturated ferrite has a dramatic effect on the parabolic-growth constant for the layer. Ignoring this flux and applying Eq. [6] would yield a value for the diffusion coefficient from the slope of the straight line in

Figure 9 that is 3.5 times as small as the actual value. This discrepancy is comparable to that found for the difference between the value for $\langle D_N^{(\gamma')} \rangle$ derived from bilayer-growth experiments using Eq. [17] and the expected value (Section V–B). Of course, for the case of a substrate of finite thickness that saturates with nitrogen during growth of the γ' layer, initially, the layer thickness increases according to the kinetics pertaining to growth into a semi-infinite substrate and during saturation changes to layer-thickness increase corresponding with growth into a saturated substrate (Figure 9).

The experimental layer-thickness data from Figure 3(b) are also given in Figure 9. In the first instance, it would be expected that these data agree with the line denoted by "finite saturating substrate." The positive deviation of the experimental data from this line is caused by the nucleation and growth stage of γ' nuclei at the surface before isolation of the substrate from the gas atmosphere, leading to the apparent nonzero layer thickness at $t = 0$ as obtained by extrapolation of the experimental parabolic-growth behavior to $t = 0$ (Section IV–A and Figure 3(b)). This stage is not accounted for in the preceding calculations.

The growth of a monolayer into a saturated substrate can be described for a nonzero layer thickness at $t = 0$ by Eq. [5], regardless of the cause for this starting condition. For a nonzero layer thickness at $t = 0$ in the cases of growth into an initially unsaturated substrate, it was found for increasing treatment time that the curve calculated for the evolution of the layer thickness approaches the one given in Figure 9 for these cases. This implies that a relatively thick layer present at $t = 0$ on an unsaturated substrate will be reduced in thickness by dissolution at the layer/substrate interface. Such a γ' layer is too thick to maintain the diffusive flux of nitrogen into ferrite by transport of nitrogen from the gas atmosphere *through* the layer. This situation can arise, for example, if a γ' monolayer is formed on an iron substrate by initially nitriding at a relatively high nitriding potential and is subsequently subjected to prolonged growth at a lower nitriding potential before saturation of the substrate has been completed. A similar situation occurs if the γ' layer has been formed in an iron substrate by high-energy ion implantation and the specimen is subsequently nitrided in a gas atmosphere.[51]

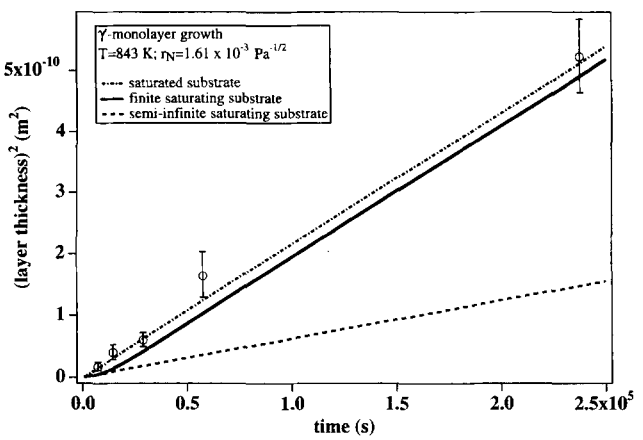

Fig. 9—The layer thickness of γ' monolayers growing into ferrite as a function of time for the nitriding conditions $T = 843$ K and $r_N = 1.61 \times 10^{-3}$ Pa$^{-1/2}$ and the (effective) diffusion coefficients $\langle D_N^{(\gamma')} \rangle = 5.97 \times 10^{-14}$ m$^2 \cdot$ s^{-1} and $D_N^{(\alpha)} = 9.93 \times 10^{-12}$ m$^2 \cdot$ s^{-1}. The substrate was considered to be saturated with nitrogen or semi-infinitely thick and initially nitrogen free or having a thickness of $8 \cdot 10^{-4}$ m and initially nitrogen free (as in the present experiments).

B. ε-Fe_2N_{1-z}/γ'-Fe_4N_{1-x} Bilayer Growth

In principle, values for the effective diffusion coefficients of nitrogen in the ε-nitride and γ'-nitride sublayers can be evaluated from Eqs. [14] and [15] and Figure 4(b). However, because of the relatively large inaccuracy in the data for the γ'-sublayer thickness, $\langle D_N^{(\varepsilon)} \rangle$ will be determined by layer-growth simulations using the calculated value of $\langle D_N^{(\gamma')} \rangle$: 7.66×10^{-14} m$^2 \cdot$ s^{-1} (Section V–B). The thickness of the sample $2L$ equals 8×10^{-4} m (Section III). In the calculations, the starting points for the sublayer thicknesses were taken as small as possible to obtain a smooth evolution for both layer thicknesses; values that were too small resulted in a chaotic or undulating evolution of both layer thicknesses on time.

The value for the effective diffusion coefficient in ε nitride was determined by trial and error such that the calculated curves in Figure 10 representing ε- and ($\varepsilon + \gamma'$)-layer growth on a saturating substrate agreed well with the experimental data for treatment times ranging from 2 to 5 hours, where porosity in the ε-layers could not be observed lightmicroscopically. It was found that $\langle D_N^{(\varepsilon)} \rangle = 4.65 \times 10^{-14}$ m$^2 \cdot$ s^{-1}. The value for $\langle D_N^{(\varepsilon)} \rangle$ obtained from direct application of Eq. [17b] to the apparent parabolic relationships in Figure 4(b), $\langle D_N^{(\varepsilon)} \rangle = 4.3 \times 10^{-14}$ m$^2 \cdot$ s^{-1} (Section V–B), deviates by only 8 pct from this numerically determined value.

For the treatment times 40 and 60 minutes the calculated ε-sublayer thickness values are slightly larger than

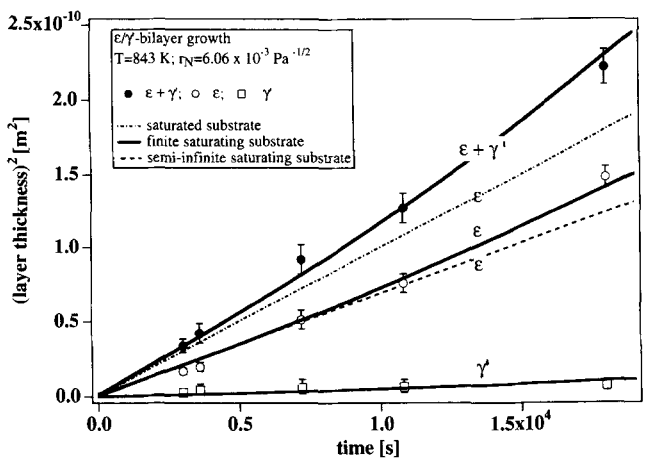

Fig. 10—The sublayer thicknesses and the total layer thicknesses of ε/γ' bilayers growing into ferrite as a function of time for the nitriding conditions $T = 843$ K and $r_N = 6.06 \times 10^{-3}$ Pa$^{-1/2}$ and the (effective) diffusion coefficient $\langle D_N^{(\varepsilon)} \rangle = 4.65 \times 10^{-14}$ m$^2 \cdot$ s^{-1}, $\langle D_N^{(\gamma')} \rangle = 7.66 \times 10^{-14}$ m$^2 \cdot$ s^{-1}, and $D_N^{(\alpha)} = 9.93 \times 10^{-12}$ m$^2 \cdot$ s^{-1}. The ε-sublayer thickness is shown for the cases that the substrate is saturated with nitrogen or semi-infinitely thick and initially nitrogen free or having a thickness of $8 \cdot 10^{-4}$ m and initially nitrogen free (as in the present experiments).

those found experimentally (Figure 10). The deviation can be attributed to the actual experimentally observed succession of stages in the development of an isolating layer: γ' nucleation followed by nucleation of ε nitride on top of γ' nuclei and, eventually, coalescence of dual-phase nuclei (Figure 5). It can therefore not be expected that the calculations agree with experiment before about 40 minutes of nitriding, corresponding with the establishment of an isolating bilayer. Further, in an initial stage of bilayer growth, the nitrogen content in ε phase at the gas/ε interface may be lower than the equilibrium nitrogen content imposed by the nitriding potential. A competition between nitrogen supply from the gas phase to the gas/ε-nitride interface and the removal of nitrogen into the specimen can occur, as discussed in Reference 36 and Section IV–A. Obviously, this effect leads to an actual thickness of the ε sublayer that is smaller than the calculated thickness.

The effects of nitrogen saturation of the substrate on the growth kinetics of the ε/γ' bilayer are shown by calculation of the sublayer thicknesses for the cases of nitrogen-saturated and semi-infinite unsaturated ferrite substrates; see Figure 10 for the absolute thickness of the ε sublayer and Figure 11 for the ratio of the sublayer-thickness values for ε nitride and γ' nitride. The value for $\langle D_N^{(\varepsilon)} \rangle$ was taken as the value determined previously. Clearly, a flux of nitrogen atoms into the substrate affects the growth kinetics of both sublayers, such that, on saturating the substrate, the thickness of the γ' sublayer increases relative to the thickness of the ε sublayer.

The case of the nucleation of an ε-nitride layer on top of an isolating γ'-nitride layer was calculated, too. After some incubation time, development of an ε-nitride layer was simulated on top of the γ' layer. Assuming that the "equilibrium" interface and surface compositions hold immediately after nucleation of the ε layer, the calculations showed that the thicknesses of the two sublayers were readily approaching the curves valid for the growth of a bilayer from zero treatment time onward: after the start of ε-sublayer growth, a reduction of the thickness of the γ'-sublayer that was produced in the stage prior to ε-nitride nucleation occurred, and a relatively rapid increase of the thickness of the ε sublayer took place. In reality, such a transition from monolayer to bilayer growth can be slower than according to the calculations, because the "equilibrium" surface composition of the ε-nitride sublayer is not likely to be attained instantaneously upon ε-nitride nucleation.

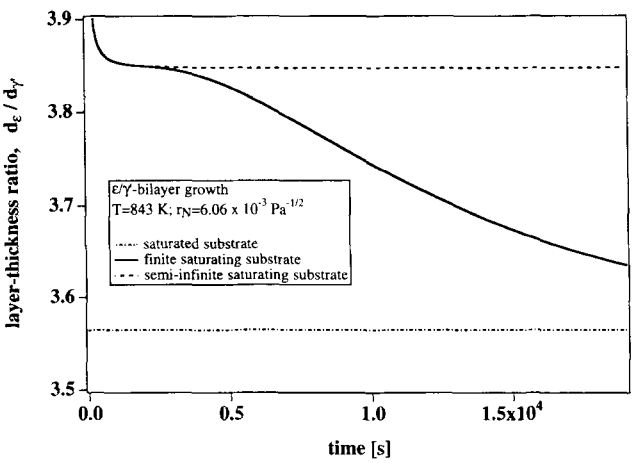

Fig. 11—Ratio of the thicknesses of the ε- and γ'-nitride sublayers, d_ε and $d_{\gamma'}$, as a function of time for the nitriding conditions T = 843 K and $r_N = 6.06 \times 10^{-3}$ $Pa^{-1/2}$ and the (effective) diffusion coefficients $\langle D_N^{(\varepsilon)} \rangle = 4.65 \times 10^{-14}$ $m^2 \cdot s^{-1}$, $\langle D_N^{(\gamma')} \rangle = 7.66 \times 10^{-14}$ $m^2 \cdot s^{-1}$, and $D_N^{(\alpha)} = 9.93 \times 10^{-12}$ $m^2 \cdot s^{-1}$. Thickness ratios are shown for the cases in which the substrate is saturated with nitrogen or semi-infinitely thick and initially nitrogen free or having a thickness of $8 \cdot 10^{-4}$ m and initially free (as in the present experiments). The initial decrease of the value for the layer-thickness ratio for the cases of a saturating substrate and the initial decrease of the value for the layer-thickness ratio for the case of a saturated substrate have no physical significance but are associated with the starting points chosen for the numerical solution of the set of differential equations (Eqs. [14] and [15]).

C. *Diffusion Coefficient of Nitrogen in ε Nitride*

The effective diffusion coefficient obtained here for the ε-nitride sublayer, $\langle D_N^{(\varepsilon)} \rangle = 4.65 \times 10^{-14}$ $m^2 \cdot s^{-1}$, is compared to values calculated by extrapolation or interpolation from reported temperature dependences in the literature:* $\langle D_N^{(\varepsilon)} \rangle = 4.3 \times 10^{-14}$ $m^2 \cdot s^{-1}$,[12] $\langle D_N^{(\varepsilon)} \rangle = 2.0 \times 10^{-14}$ $m^2 \cdot s^{-1}$,[13] and $\langle D_N^{(\varepsilon)} \rangle = 3.4 \times 10^{-14}$ $m^2 \cdot s^{-1}$.[50] These values differ by a factor of 1 to 2. Obviously, the analysis in Section II–B (Eqs. [12] and [19]) shows that at least part of the differences between the values for $\langle D_N^{(\varepsilon)} \rangle$ is due to (1) different models used to evaluate the diffusion coefficients from layer-growth experiments, and (2) different values for the surface and interface compositions used for the calculation of values for a diffusion coefficient for nitrogen in ε nitride from the layer-growth experiments in the various studies. Further, the value for $\langle D_N^{(\varepsilon)} \rangle$ as given in Reference 12 was evaluated from nitriding experiments performed on a steel substrate. The possible uptake of carbon in the ε layer and its effect on the nitrogen activity was not accounted for. Moreover, in Reference 12 the determination of the nitrogen concentration-depth profile was rather imprecise (wet-chemical analysis of small flakes taken at different depths in the compound layer).

*The diffusion coefficients given in the literature are taken as effective diffusion coefficients and are based on models not always known to us. This hinders a fair comparison of values for the diffusion coefficient. It is emphasized that on application of a particular diffusion coefficient, the corresponding model that was used to evaluate the diffusion coefficient should be considered.

For practical purposes, the effective diffusion coefficient of nitrogen in ε nitride should be available in a wide range of compositions and temperatures. Hence, an evaluation of the self-diffusion coefficient of nitrogen in ε nitride and its dependence on composition and temperature is necessary, requiring extensive experimental work. The model given by Eqs. [14] and [15] and the procedure based on a combination of monolayer- and bilayer-growth experiments at several nitriding potentials as applied in the present article provide a route for the determination of the desired kinetic data.

The self-diffusion coefficient at 843 K can be determined from the present experiments using Eq. [19] and the data in Eqs. [A8], [A9], and [A15]: $D_N^{(\varepsilon)*} = 12.6 \times 10^{-15}$ $m^2 \cdot s^{-1}$. This value is 12.3 times as large as the value obtained for self-diffusion in γ'-nitride layers at

the same temperature (Table II). This difference will be discussed in Section VII.

VII. ATOMISTIC MECHANISMS OF DIFFUSION IN ε AND γ' NITRIDE

In ε and in γ' nitrides, the nitrogen atoms reside in a more (γ') or less (ε) ordered way on their sublattice constituted by all octahedral interstices of the hcp and the fcc sublattices of iron atoms: order sites and disorder sites can be discerned in the nitrogen sublattices. Then, diffusion of the nitrogen atoms on their own sublattice is possible by three mechanisms:

(1) diffusion over disorder sites only,
(2) diffusion over order sites only, or
(3) diffusion over both order and disorder sites.

For all of these cases, the migration from one site of the nitrogen sublattice to the other proceeds *via* a tetrahedral interstice of the iron sublattice. In view of the ground-state structures (types of ordering) observed for ε and γ' nitrides[48] all three mechanisms can be operative for ε nitride, whereas only mechanisms 1 and 3 can occur for γ' nitride, *i.e.*, nitrogen diffusion in γ' nitride always involves use of disorder sites. A high diffusion rate requires a reasonable occupancy of disorder sites and a reasonable fraction of vacant order sites.

Recently, the thermodynamics of long-range order of nitrogen in ε and γ' nitrides was successfully described[21] (Appendix). The occupancies of the sites of the sublattices for nitrogen in ε and γ' nitrides were calculated, and it was found that the fraction of the disorder sites that is occupied by nitrogen atoms is very small for γ' nitride as compared to ε nitride. Further, the fraction of vacant order sites is also much smaller for γ'-nitride than for ε nitride: the degree of order of the nitrogen atoms in γ' nitride is considerably higher than the degree(s) of order of the nitrogen atoms in ε nitride.[21,44] The distance between two sites of the nitrogen sublattice involved in migration is different for the two nitrides. For ε nitride, site separation in the direction perpendicular to the basal plane of the hexagonal unit cell is smaller than the separation between neighboring sites within the basal plane; for γ' nitride, site separation is the same in all directions and of about the same magnitude as site separation in the basal plane of the hexagonal unit cell of ε nitride. All elements of the preceding discussion suggest faster migration of nitrogen in ε nitride relative to γ' nitride and, thus, may explain a self-diffusion coefficient of nitrogen in ε nitride that is larger than the self-diffusion coefficient of nitrogen in γ' nitride.

Further, $D_N^{(\varepsilon)*}$ is likely to depend on the composition, because within the relatively broad homogeneity range of ε nitride, (1) the ground-state structure according to which the nitrogen atoms are ordered changes with variation of nitrogen content and (2) the degree(s) of order in the ground-state structures increase(s) with increasing nitrogen content.[44] For the present experiments, it is likely that the composition dependency of $D_N^{(\varepsilon)*}$ can be omitted, because the composition range of the ε-nitride layers was relatively small as compared to the homogeneity range and such that only one type of ordering could occur (denoted as configuration B.[44])

In principle, for ε nitride, because of its hexagonal unit cell, a crystallographic orientation dependence of the self-diffusion coefficient of nitrogen is expected with two principal self-diffusion coefficients in two mutually perpendicular directions, *i.e.*, parallel to and perpendicular to the basal planes. So far, the development of pronounced crystallographic texture resulting from growth selection by preferred growth of a specific crystallographic orientation, as, for example, observed for boride layers,[31] has not been observed for ε-nitride layers. This suggests that the principal self-diffusion coefficients do not differ much. Note that diffusion in the direction of shortest site separation, *i.e.*, in the direction perpendicular to the basal plane, implies migration in the direction of strongest pairwise interaction of neighboring nitrogen atoms;[44] these factors have antagonistic effects on the probability of migration in this direction.

VIII. CONCLUSIONS

Models have been presented for the diffusion-controlled growth of mono- and bilayers into a substrate with concentration-dependent diffusion coefficients of the (main) diffusing component in (each of) the sublayer(s). For the case that solute diffusion is rate determining, the effective diffusion coefficient is taken as the corresponding intrinsic diffusion coefficient weighted over the composition range of the layer.

A. *Layer-Growth Kinetics on Gaseous Nitriding of Iron*

On nitriding ferritic iron, the development of γ'-Fe_4N_{1-x} monolayers and of ε-Fe_2N_{1-z}/γ'-Fe_4N_{1-x} bilayers at the surface of the substrate is preceded by the dissolution of nitrogen into the ferrite substrate. After exceeding the maximal solubility of nitrogen in ferrite at the surface, γ'-Fe_4N_{1-x} nucleates there. The γ' nuclei grow both laterally and into the ferrite, coalesce, and, eventually, establish a layer at the surface that isolates the nitriding medium from the ferrite substrate. Prior to isolation, diffusion of nitrogen *via* ferrite toward the γ' nuclei may contribute to the growth of these nuclei. If the nitriding potential allows the development of ε nitride, this nitride nucleates on the top of γ' nitride, even before isolation of the substrate from the nitriding medium has occurred. The thicknesses of the nitride (sub)layers constituting the mono- and bilayers grow parabolically with the nitriding time. The development of porosity resulting from the precipitation of N_2-gas in, especially, the surface-adjacent part of the ε sublayer leads to "blowing up" of the ε-sublayer thickness and, after the coalescence of pores to channels connecting the interior with the nitriding medium, to the uptake of nitrogen at channel surfaces. In this stage of nitriding, the ε sublayer grows faster than prescribed by the parabolic rate law in the preceding stage.

B. *Diffusion Coefficients for Nitrogen in Iron Nitrides*

Layer-growth simulations showed that the dissolution of nitrogen in an initially unsaturated ferrite substrate strongly retards the growth rate of a γ' monolayer as well as the growth rate of an ε/γ' bilayer.

1. γ'-Fe_4N_{1-x}

The value obtained for the self-diffusion coefficient of nitrogen in γ'-nitride, $D_N^{(\gamma')*}$, is in good agreement with data taken from the literature and re-evaluated in the present article. It was obtained ($D_N^{(\gamma')*}$ in $m^2 \cdot s^{-1}$; T in K)

$$\ln D_N^{(\gamma')*} = -\frac{91.4 \times 10^3}{RT} - 21.7 \quad \text{for } 777\ \text{K} < T < 843\ \text{K}$$

The intrinsic diffusion coefficient of nitrogen in γ' nitride depends strongly on the nitrogen concentration, because the thermodynamical factor changes strongly with the composition.

2. ε-Fe_2N_{1-z}

The value obtained for the self-diffusion coefficient of nitrogen in ε nitride at 843 K is $D_N^{(\varepsilon)*} = 12.6 \times 10^{-15}\ m^2 \cdot s^{-1}$. This value is about 12 times as high as the value for the self-diffusion coefficient of nitrogen in γ' nitride at 843 K: $D_N^{(\gamma')*} = 10.2 \times 10^{-16}\ m^2 \cdot s^{-1}$. The difference can be ascribed to a lower degree of order for the nitrogen atoms on the hexagonal nitrogen sublattice in ε nitride, as compared to the nitrogen atoms on the cubic nitrogen sublattice in γ' nitride.

APPENDIX

Thermodynamic and crystallographic data for Fe-N phases

This appendix summarizes thermodynamic and crystallographic data of the Fe-N phases α-Fe, γ-Fe_4N_{1-x}, and ε-Fe_2N_{1-z} for temperatures below the eutectoid temperature of 863 K that was used in the calculations presented in this article.

Concentration values c_j of nitrogen in phase j (in $mole \cdot m^{-3}$) were calculated from

$$c_j = \frac{1}{N_{Av}} \cdot \frac{N_j}{1 - N_j} \cdot \frac{1}{V_j} = \frac{n}{N_{Av}} \cdot y_{N,j} \cdot \frac{1}{V_j} \qquad [A1]$$

where N_j is the atomic fraction of nitrogen, n is the number of sites of the nitrogen sublattice, constituted by all octahedral interstices of the iron sublattice relative to the number of sites of the iron sublattice (for bcc $n = 3$; for fcc and hcp, $n = 1$), $y_{N,j}$ is the nitrogen content expressed as the fractional occupancy of the nitrogen sublattice in phase j, V_j is the volume of the unit cell of phase j per iron atom, and N_{Av} is Avogadro's number. The volume of the unit cell of phase j was calculated from the dependence of the corresponding lattice parameter on nitrogen content (at room temperature).

The nitrogen contents at the surface were derived from absorption isotherms giving, for a particular phase j, the dependence of equilibrium nitrogen content on the nitriding potential r_N at a specific temperature. Those at the interphase interfaces (*i.e.*, α/γ', γ'/α, γ'/ε, and ε/γ' interfaces) were obtained from the corresponding phase boundaries in the Fe-N phase diagram.

Thermodynamic Data

The thermodynamic data for Fe-N phases were taken from a recent compilation and evaluation.[21] The equilibrium between the solid Fe-N phase and an ammonia/hydrogen gas mixture is the basis for the thermodynamical considerations:

$$NH_3 \rightleftarrows N_j + \frac{3}{2} H_2 \qquad [A2]$$

where N_j denotes nitrogen dissolved in phase j on its own sublattice. Hence, the equilibrium constant reads

$$K_j = \frac{a_{N_j} \cdot f_{H_2}^{3/2}}{f_{NH_3}} \qquad [A3]$$

where a_{N_j} is the activity of occupied sites of the nitrogen sublattice and f_{H_2} and f_{NH_3} are the fugacities of hydrogen and ammonia, respectively. Here the fugacities, f_k, are taken as proportional to corresponding partial pressures, p_j, implying constant fugacity coefficients (for ideal gases fugacities are identical to partial pressures).

Absorption isotherms

An absorption isotherm provides the relation between the nitrogen content, $y_{N,j}$, and the nitriding potential, r_N ($=pNH_3/pH_2^{3/2}$).

α-Fe

The nitrogen-absorption isotherms for α-Fe show a linear relation between $y_{N,\alpha}$ and r_N. Hence, the activity coefficient γ in $a_{N_j} = \gamma \cdot y_{N,\alpha}$ is constant, *i.e.*, Henry's law is obeyed. Thus, it follows from Eq. [A3] that

$$y_{N,\alpha} = K'_\alpha \cdot r_N \qquad [A4]$$

where K'_α contains the equilibrium constant for the gas/ferrite equilibrium and the various activity and fugacity coefficients. Averaging the results from References 9 and 41,[21] the following equation is obtained for the temperature dependence of K'_α

$$\ln \frac{y_{N,\alpha}}{r_N} = -\frac{9096}{T} + 11.56 \qquad [A5]$$

where r_N is given in $Pa^{-1/2}$ and T is the absolute temperature in K.

γ'-Fe_4N_{1-x}

The nitrogen-absorption isotherms for γ' nitride can be adequately described by Wagner–Schottky isotherms[20,42]

$$y_{N,\gamma'} = \frac{1}{4}\left(1 + K_{\gamma'}^{WS}\left[\frac{r_N}{r_{N,\gamma'}^0} - \frac{r_{N,\gamma'}^0}{r_N}\right]\right) \qquad [A6]$$

where $K_{\gamma'}^{WS}$ is an equilibrium constant not to be confused with $K_{\gamma'}$ (for physical interpretation, see References 20 and 21), and $r_{N,\gamma'}^0$ is the hypothetical nitriding potential necessary to obtain a nitrogen content corresponding with the stoichiometric composition Fe_4N. Using the data provided in References 20 and 9, the following equations were obtained[21]

$$\ln K_{\gamma'}^{WS} = -\frac{7558}{T} + 2.978 \qquad [A7a]$$

$$\ln r_{N,\gamma'}^0 = \frac{6352}{T} - 12.45 \qquad [A7b]$$

where $r_{N,\gamma'}^0$ is expressed in $Pa^{-1/2}$.

ε-Fe_2N_{1-z}

Experimental nitrogen-absorption isotherms for ε-nitride[10] were recently shown to be in very good agreement with predictions from a long range order model (LRO model) for interstitials in an hcp lattice.[44] For compositions of ε within the range $0.25 < y_{N,\varepsilon} < 0.43$, the numerical results of the LRO model can be represented accurately by[21]

$$\ln\left(\frac{r_N}{r^0_{N,\varepsilon}}\right) = -7.07 - 8.01\, y_{N,\varepsilon} + 41.1\, y^2_{N,\varepsilon} \quad [A8]$$

The nitriding potential $r^0_{N,\varepsilon}$ cannot be interpreted in a similarly straightforward way as $r^0_{N,\gamma'}$ (for a full discussion, see Reference 21). The following equation was obtained[21]

$$\ln r^0_{N,\varepsilon} = \frac{3330}{T} - 4.377 \quad [A9]$$

with $r^0_{N,\varepsilon}$ in $Pa^{-1/2}$.

Nitriding potentials at phase boundaries

The nitriding potentials where two coexisting phases i and j are in equilibrium with the gas mixture are denoted here as phase boundary nitriding potentials, $r_{N,i/j}$. The dependencies of these equilibrium values for $r_{N,i/j}$ on temperature were given firstly by Lehrer.[45] Here, the descriptions given in Reference 21 are used.

$$\alpha/\gamma' \textit{ equilibrium}: \ln r_{N,\alpha/\gamma'} = \frac{4555}{T} - 12.88 \quad [A10]$$

and

γ'/ε *equilibrium*:

$$\ln r_{N,\gamma'/\varepsilon} = \sqrt{\frac{60{,}536}{T} - 56.85} - 9.63 \quad [A11]$$

with $r_{N,i/j}$ in $Pa^{-1/2}$.

Composition at phase boundaries

The phase boundaries $\alpha/\alpha + \gamma'$, $\alpha + \gamma'/\gamma'$, $\gamma'/\gamma' + \varepsilon$, and $\gamma' + \varepsilon/\varepsilon$ in the Fe-N phase diagram were evaluated from Eqs. [A5] through [A11]. The following equations were obtained:

$$\alpha/\alpha + \gamma': \ln y_{N,\alpha} = -\frac{4541}{T} - 1.32 \quad [A12]$$

$$\alpha + \gamma'/\gamma': \ln(1 - 4y_{N,\gamma'}) = -\frac{7558}{T} + 2.978 + \ln\left(\frac{r^0_{N,\gamma'}}{r_{N,\alpha/\gamma'}} - \frac{r_{N,\alpha/\gamma'}}{r^0_{N,\gamma'}}\right) \quad [A13]$$

where $r_{N,\alpha/\gamma'}$ and $r^0_{N,\gamma'}$ are given by Eqs. [A10] and [A7b], respectively.

$$\gamma'/\gamma' + \varepsilon: \ln(1 - 4y_{N,\gamma'}) = -\frac{7558}{T} + 2.978 + \ln\left(\frac{r^0_{N,\gamma'}}{r_{N,\gamma'/\varepsilon}} - \frac{r_{N,\gamma'/\varepsilon}}{r^0_{N,\gamma'}}\right) \quad [A14]$$

where $r_{N,\gamma'/\varepsilon}$ and $r^0_{N,\gamma'}$ are given by Eqs. [A11] and [A7b], respectively.

$$\gamma' + \varepsilon/\varepsilon: -8.01\, y_{N,\varepsilon} + 41.1\, y^2_{N,\varepsilon} = -\frac{3330}{T} + 1.817 + \sqrt{\frac{60{,}536}{T} - 56.85} \quad [A15]$$

The $\alpha/\alpha + \gamma'$, $\alpha + \gamma'/\gamma'$, and $\gamma'/\gamma' + \varepsilon$ interface compositions as represented by Eqs. [A12] throughout [A14] are more accurate than the experimental interface compositions (cf. discussion in Ref. 21). On the other hand, the $\gamma' + \varepsilon/\varepsilon$-interface composition, as represented by Eq. [A15], is very sensitive to small changes of the nitriding potential, and therefore, the experimentally determined phase compositions are more accurate.[21] In calculating the effective diffusion coefficient and the self-diffusion coefficient, as in the present article, accurate values for the compositions at the interfaces are a prerequisite. Therefore, here the composition of ε nitride at the $\gamma' + \varepsilon/\varepsilon$ phase boundary was evaluated from interpolation among experimental data. It was found by least-squares fitting

$$\gamma' + \varepsilon/\varepsilon: \frac{y_{N,\varepsilon}}{1 + y_{N,\varepsilon}} = 5.758 \times 10^{-2} + 6.621 \times 10^{-4}\, T - 5.345 \times 10^{-7}\, T^2 \quad [A16]$$

Crystallographic Data

α-Fe

The lattice parameter of α-Fe (bcc sublattice of iron atoms), a_α, depends on the nitrogen content, according to Reference 46:

$$a_\alpha = 0.28663 + 0.20505\, y_{N,\alpha} \quad \text{(nm)}$$

The volume of the unit cell per iron atom:
$V_\alpha = 1/2\ a^3_\alpha$.

γ'-Fe_4N_{1-x}

The lattice parameter of γ'-Fe_4N_{1-x} (fcc sublattice of iron atoms), $a_{\gamma'}$, depends on the nitrogen content according to Reference 33:

$$a_{\gamma'} = 0.37988 + 0.095315\left(y_{N,\gamma'} - \frac{1}{4}\right) \quad \text{(nm)}$$

The volume of the unit cell per iron atom:
$V_{\gamma'} = 1/4\ a^3_{\gamma'}$.

ε-Fe_2N_{1-z}

The lattice parameters of ε nitride (hcp sublattice of iron atoms), a_ε and c_ε, referring to the Fe sublattice, were evaluated in Reference 47 from a survey of literature data. Recognizing that the incorporation of long-range ordering of nitrogen atoms in ε nitride implies the definition of a unit cell with lattice parameters a'_ε and c'_ε; with $a'_\varepsilon = a_\varepsilon\sqrt{3}$, and $c'_\varepsilon = c_\varepsilon$,[48] it was obtained in Reference 47 that

$$\alpha'_\varepsilon = a_\varepsilon \sqrt{3} = 0.43535 + 0.1337 \frac{y_{N,\varepsilon}}{1 + y_{N,\varepsilon}} \quad \text{(nm)}$$

and

$$c'_\varepsilon = c_\varepsilon = 0.423321 + 0.0578 \frac{y_{N,\varepsilon}}{1 + y_{N,\varepsilon}} \quad \text{(nm)}$$

The volume of the unit cell per iron atom:
$V_\varepsilon = 1/4\ a_\varepsilon^2 \cdot c_\varepsilon \sqrt{3}$.

ACKNOWLEDGMENTS

The work in the present article was initiated February 1984 and was part of the Master's Thesis (Delft University of Technology, 1985) of one of the authors (MAJS). It was not published until now because of lack of accurate interface-composition and absorption-isotherm data for the nitride layers. Over the years, several people have contributed. We are obliged to Dr. H.C.F. Rozendaal and Professor B.M. Korevaar for stimulating discussions and constructive criticism in an early stage of the project. P.J. van der Schaaf is thanked for skillful technical assistance with the nitriding experiments. We are grateful to Ir. W.G. Sloof for the EPMA measurements and to Ir. B.J. Kooi for assistance with the evaluation of the data given in the Appendix.

These investigations in the program of the Foundation for Fundamental Research of Matter (FOM) have been supported (in part) by the Netherlands Technology Foundation (STW). Financial support from PBTS and IOP-Metalen is gratefully acknowledged.

REFERENCES

1. T. Bell: *Heat Treat. Met.*, 1975, vol. 2, pp. 39-49.
2. K. Sachs and D.B. Clayton: *Heat Treat. Met.*, 1979, vol. 6, pp. 29-34.
3. Ya.D. Kogan and A.A. Bulgach: *Metalloved. Term. Obrab. Met.*, 1984, vol. 13, pp. 10-20.
4. W. Jentzsch and S. Böhmer: *Neue Hütte*, 1979, vol. 24, pp. 249-53.
5. E. Metin, A.D. Romig Jr., O.T. Inal, and R.E. Semarge: in *Microbeam Analysis 1988*, D.E. Newbury, ed. San Francisco Press Inc., San Francisco, CA, 1989, pp. 498-502.
6. D. Heger and D. Bergner: *Härterei-Tech. Mitt.*, 1990, vol. 46, pp. 331-38.
7. Hong Du and J. Ågren: *Mater. Sci. Forum*, 1992, vol. 102-104, pp. 243-48.
8. A. Marciniak: *Surf. Eng.*, 1985, vol. 1, pp. 283-88.
9. Z. Przylecki and L. Maldzinski: in *Carbides, Nitrides and Borides*, Poznan/Kolobrzeg, Poznan, Poland, 1987, pp. 153-162.
10. L. Maldzinski, Z. Przylecki, and J. Kunze: *Steel Res.*, 1986, vol. 12, pp. 646-50.
11. K. Schwerdtfeger, P. Grieveson, and E.T. Turkdogan: *Trans. AIME*, 1969, vol. 245, pp. 2461-466.
12. B. Prenosil: *Kovove Mater.*, 1965, vol. 3, pp. 69-87.
13. Yu.M. Lakhtin and Ya.D. Kogan: *Nitriding of Steel*, [(in Russian)] Mashinostroenie, Moscow, 1976.
14. L.S. Darken: *Trans. AIME*, 1948, vol. 175, pp. 184-94.
15. M.A.J. Somers and E.J. Mittemeijer: *Surf. Eng.*, 1987, vol. 3, pp. 123-37.
16. W. Jost: *Diffusion in Solids, Liquids and Gases*, Academic Press Inc., New York, NY, 1960, pp. 71-72.
17. S. Crusius, G. Inden, U. Knoop, L. Höglund, and J. Ågren: *Z. Metallkd.*, 1992, vol. 83, pp. 673-78.
18. J. Crank: *The Mathematics of Diffusion*, Clarendon Press, Oxford, 1956.
19. J. Colwell, G.W. Powell, and J.L. Ratliff: *J. Mater. Sci.*, 1977, vol. 12, pp. 543-48.
20. H.J. Grabke: *Ber. Bunsengesell, Phys. Chem.*, 1969, vol. 73, pp. 596-601.
21. B.J. Kooi, M.A.J. Somers, and E.J. Mittemeijer: Delft University of Technology, Delft, The Netherlands, unpublished research, 1993.
22. G.V. Kidson: *J. Nucl. Mater.*, 1961, vol. 3, pp. 21-29.
23. C. Wagner: *Acta Metall.*, 1969, vol. 17, pp. 99-107.
24. A.J. Hickl and R.W. Heckel: *Metall. Trans. A*, 1975, vol. 6A, pp. 431-40.
25. A.K. Sarkhell and L.L. Seigle: *Metall. Trans. A*, 1976, vol. 7A, pp. 899-902.
26. S.R. Shatynski, J.P. Hirth, and R.A. Rapp: *Acta Metall.*, 1976, vol. 24, pp. 1071-78.
27. D.S. Williams, R.A. Rapp, and J.P. Hirth: *Metall. Trans. A*, 1981, vol. 12A, pp. 639-52.
28. Guan-Xing Li and G.W. Powell: *Acta Metall.* 1985, vol. 33, pp. 23-31.
29. E. Fromm: *Z. Metallkd.*, 1966, vol. 57, pp. 60-65.
30. U. Roy: *Acta Metall.*, 1968, vol. 16, pp. 243-53.
31. C.M. Brakman, A.W.J. Gommers, and E.J. Mittemeijer: *J. Mater. Res.*, 1989, vol. 4, pp. 1354-70.
32. A. Wells: *J. Mater. Sci.*, 1985, vol. 20, pp. 2439-445.
33. M.A.J. Somers, N.M. van der Pers, D. Schalkoord, and E.J. Mittemeijer: *Metall. Trans. A*, 1989, vol. 20A, pp. 1533-539.
34. G.F. Bastin, H.J.M. Heijligers, and F.J.J. van Loo: *Scanning*, 1984, vol. 6, pp. 58-68.
35. J.R.G. da Silva and R.B. McLellan: *Mater. Sci. Eng.*, 1976, vol. 26, p. 83.
36. H.C.F. Rozendaal, E.J. Mittemeijer, P.F. Colijn, and P.J. van der Schaaf: *Metall. Trans. A*, 1983, vol. 14A, pp. 395-99.
37. E.J. Mittemeijer, M. van Rooijen, I. Wierzyllowski, H.C.F. Rozendaal, and P.F. Colijn: *Z. Metallkd.*, 1983, vol. 74, pp. 473-83.
38. M.A.J. Somers and E.J. Mittemeijer: *Metall. Trans. A*, 1990, vol. 21A, pp. 189-204.
39. Liu Cheng and E.J. Mittemeijer: *Metall. Trans. A*, 1990, vol. 21A, pp. 13-26.
40. M.A.J. Somers and E.J. Mittemeijer: *Metall. Trans. A*, 1990, vol. 21A, pp. 901-12.
41. H.H. Podgurski and H.W. Knechtel: *Trans. AIME*, 1969, vol. 245, pp. 1595-1602.
42. H.A. Wriedt: *Trans. AIME*, 1969, vol. 245, pp. 43-46.
43. H.J. Grabke: *Ber. Bunsengesell. Phys. Chem.*, 1968, vol. 72, pp. 533-48.
44. B.J. Kooi, M.A.J. Somers, and E.J. Mittemeijer: *Metall. Mater. Trans. A*, in press.
45. E. Lehrer: *Z. Electrochem.*, 1930, vol. 36, pp. 383-92.
46. P. Ferguson and K.H. Jack: *Proc. Heat Treatment '81*, The Metals Society, London, 1981, pp. 158-63.
47. D. Firrao, B. DeBenedetti, and M. Rosso: *Metall. Ital.*, 1979, vol. 71, p. 373.
48. K.H. Jack: *J. Appl. Cryst.*, 1952, vol. 5, pp. 404-11.
49. B. Pieraggi: *Oxid. Met.*, 1987, vol. 27, pp. 177-185.
50. L. Torchane, P. Bilger, J. Dulcy, and M. Gantois: *Mater. Sci. Forum*, 1994, vol. 163–165, pp. 707-12.
51. A.M. Vredenberg: Ph.D. Thesis, University of Utrecht, 1991.